Atlantic Water intrusion triggers rapid retreat and regime change at previously stable Greenland glacier

Thomas R. Chudley
Byrd Polar and Climate Research Center, Ohio State University, Columbus, OH, USA
https://orcid.org/0000-0001-8547-1132

Ian M. Howat
Byrd Polar and Climate Research Center, Ohio State University, Columbus, OH, USA
School of Earth Sciences, Ohio State University, Columbus, OH, USA
https://orcid.org/0000-0002-8072-6260

Michalea D. King
Polar Science Center, University of Washington, Seattle, WA, USA
https://orcid.org/0000-0002-8138-4362

Adelaide Negrete
Byrd Polar and Climate Research Center, Ohio State University, Columbus, OH, USA

Correspondence: Tom Chudley (chudley.1@osu.edu)

Atlantic Water intrusion triggers rapid retreat and regime change at previously stable Greenland glacier

Chudley, T. R.[1]*, Howat, I. M.[1,2], King, M. D.[3], Negrete, A.[1]

[1] Byrd Polar and Climate Research Center, Ohio State University, Columbus, OH, USA
[2] School of Earth Sciences, Ohio State University, Columbus, OH, USA
[3] Polar Science Center, University of Washington, Seattle, WA, USA

Correspondence: Tom Chudley (chudley.1@osu.edu)

Abstract

Ice discharge from Greenland's marine-terminating glaciers contributes to half of all mass loss from the ice sheet, with numerous mechanisms proposed to explain their retreat. Here, we examine K.I.V Steenstrups Nordre Bræ ('Steenstrup') in Southeast Greenland, which, between 2018—2021, retreated ~7 km, thinned ~20%, doubled in discharge, and quadrupled in flow speed. This rate of acceleration is unprecedented amongst Greenland's glaciers, and now places Steenstrup in the top 10% of glaciers by contribution to Greenland's discharge. In contrast to expected behaviour from a shallow, grounded tidewater glacier, Steenstrup was insensitive to high surface temperatures that destabilised many regional glaciers in 2016, responding instead to a large anomaly in deeper Atlantic Water (AW) in 2018. By 2021, a rigid pro-glacial mélange had developed alongside notable seasonal variability. Steenstrup's behaviour highlights that even apparently long-term stable glaciers with high sills are vulnerable to sudden and rapid retreat from warm AW intrusion.

1. Introduction

The Greenland Ice Sheet is the dominant contributor to global sea-level rise from the cryosphere, losing 222 ± 30 billion tonnes of ice per year between 2012 and 2017 (IMBIE Team, 2020). Between a half and two-thirds of loss since the 1990s has been attributed to acceleration in ice discharge from marine-terminating outlet glaciers (IMBIE Team, 2020; Mouginot *et al.* 2019, King *et al.* 2020), a process initiated through interactions between the ocean and the glacier terminus (e.g. Holland *et al.* 2008; Straneo and Heinbach, 2013; Catania *et al.* 2020). Understanding these interactions is a critical component of understanding future sea level contributions from the Greenland Ice Sheet (Catania *et al.* 2020).

Forcing at the ice-ocean interface is understood to occur via two primary mechanisms. The first is the submarine melting of glacier termini. This is forced by the transport of warm, deep Atlantic Water (AW) through fjords to glacier calving fronts (Seale *et al.* 2011, Straneo and Heinbach, 2013, Slater *et al.* 2020), initiating calving loss by submarine melt and undercutting of the ice front (Xu *et*

al. 2013; Rignot *et al.* 2016; Wood *et al.* 2018; 2021). Heat transfer between the ocean and ice is enabled by near-ice circulation and plumes from fresh subglacial discharge (Slater *et al.* 2018, Fried *et al.*, 2015), which is sourced from surface melt of the ice sheet, leading to both oceanic and atmospheric influences on terminus melting (Slater and Straneo, 2022). The second mechanism is the modulation of calving rate via rigid ice mélange (Walter *et al.* 2012; Cassotto *et al.* 2015; Moon *et al.* 2015; Bevan *et al.* 2019; Joughin *et al.* 2020; Fried *et al.* 2018), the backstress of which acts to inhibit calving (Burton *et al.* 2018, Todd *et al.* 2018; Schlemm and Levermann, 2021) and can be reduced in response to warm surface waters (Bevan *et al.* 2019, Barrett *et al.* 2022). Both mechanisms have the potential to trigger rapid retreat in previously stable glaciers, sustained by positive feedbacks arising from retrograde bed slopes (Catania *et al.* 2018) and dynamic thinning (Felikson *et al.* 2017, Cassotto *et al.* 2019).

However, glaciers exhibit highly heterogeneous responses to relatively uniform ocean forcing (King *et al.* 2020; Mouginot *et al.* 2019), even when directly adjacent (e.g. McFadden *et al.* 2011, An *et al.* 2021, Carr *et al.* 2014). This variability has been attributed to fjord geometry (Wood *et al.* 2021, Millan *et al.* 2018), glacier geometry (Enderlin *et al.* 2013, Morlhigem *et al.* 2016, Felikson *et al.* 2017, Todd *et al.* 2018), subglacial hydrology (Bartholomaus *et al.* 2016), and the distribution of oceanographic currents (Seale *et al.* 2011; Walsh *et al.* 2012). None of these, however, can consistently explain spatio-temporal heterogeneity in glacier response, suggesting that such variability is a complex combination of multiple conditions. For instance, some have argued that deep termini, susceptible to buoyant flexure and losing mass through full-thickness calving, are controlled by seasonal (Moon *et al.* 2015) and inter-annual (Bevan *et al.* 2019) mélange variability, whilst retreat of shallow glaciers, calving primarily through small-magnitude serac failure, is driven primarily by subglacial melt (Fried *et al.* 2018; Catania *et al.* 2020). Conversely, others have suggested that the deep termini are forced by AW intrusion, whilst shallow, well-grounded glaciers are protected by their proglacial bathymetry (Millan *et al.* 2018; Wood *et al.* 2021, Jakobsson *et al.* 2020). The former has been supported by glacier-scale studies of deep outlets such as Sermeq Kujalleq (Jakobshavn Isbræ) and Kangerlussuaq (Joughin *et al.* 2020, Bevan *et al.* 2019, Barnett *et al.* 2022), which conclude that retreat was initiated by the destabilisation of rigid winter mélange. Meanwhile, other studies have found deep outlets such as Zachariae Isstrøm (An *et al.* 2021) and Helheim (Straneo and Heimbach, 2013), to be forced primarily by AW. Todd *et al.* (2019) found Sermeq Kujalleq (Store Glacier) susceptible to both processes, destabilising entirely in response to either a doubling of frontal melt or a complete loss of mélange. This is problematic for larger-scale modelling exercises, which frequently choose only one mode of ice-ocean interaction to parameterise (Morlighem *et al.* 2019, Slater *et al.* 2020). Being able to better diagnose the controls on tidewater glacier vulnerability is important as many glaciers that contribute significantly to Greenland's cumulative ice discharge are less well studied than the few that dominate the literature (Mouginot *et al.* 2019).

This diverse forcing has typified Greenland's southeast sector. A dramatic increase in ice discharge beginning in ~2001 that extended as far as 69°N was attributed to AW (Seale *et al.* 2011; Straneo and Heinbach, 2013; Wood *et al.* 2021), corresponding with the latitudinal extent of the warm subtropical waters carried by the Irminger Current (Seal *et al.* 2011; Walsh *et al.* 2012). Retreating glaciers were typified by deep fjords (allowing AW access) and retrograde bedslopes (Millan *et al.* 2018). However, a more recent synchronised retreat in response to atmospheric warming began across the sector in 2016 (Liu *et al.* 2022), including at Kangerlussuaq (Bevan *et al.* 2019; Brough *et al.* 2019). Studies of ocean reanalysis data concluded that this response was

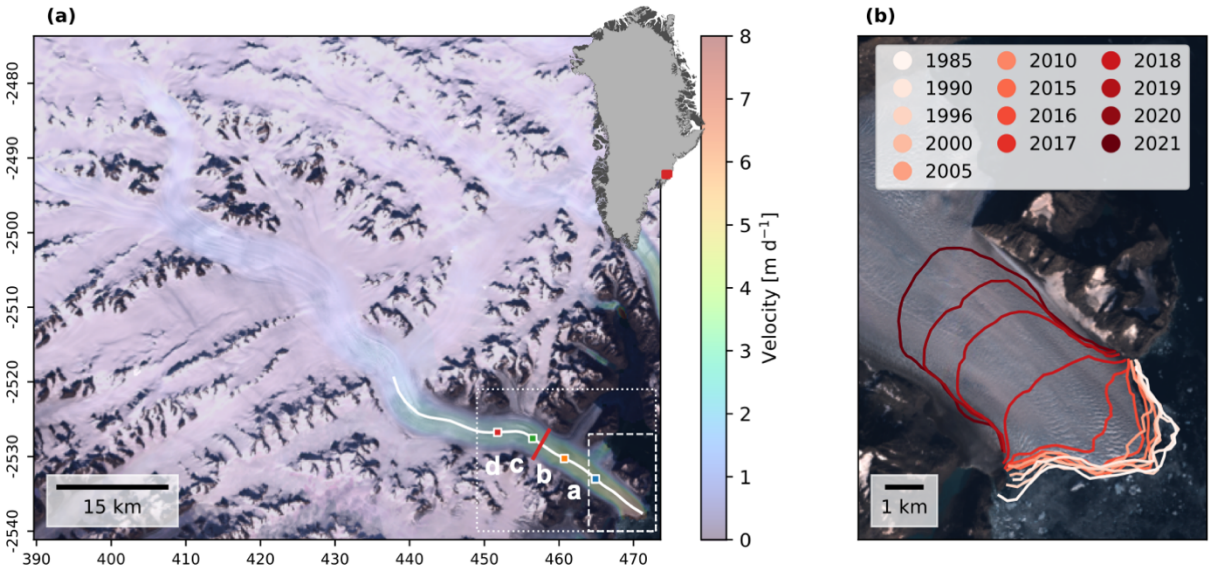

Figure 1: *(a) Location and speed of KIV Steenstrup Nordre Bræ. Colour scale indicates the mean 2016 velocity from ITS_LIVE velocity pairs. Coloured squares a-d indicate locations used to sample velocity time-series in fig. 2, white line marks centreline used to derive profiles in fig. 3, and red line marks the flux gate used for ice discharge calculation. Dotted box marks extent of fig. 4 and dashed box marks extent of panel b. Background is a composite of median Sentinel-2 RGB pixel values May–October 2016. Coordinates in unit kilometres of NSIDC Polar Stereographic North. Inset shows location of Steenstrup within Greenland. (b) Changing front position of Steenstrup since 2016, identified using GEEDiT (Lea et al. 2019).*

not due to AW, which experienced no anomaly in 2016 (Bevan *et al.* 2019; Liu *et al.* 2022). Instead, it was proposed that the retreats occurred in response to either (i) atmospheric forcing leading to a high cumulative meltwater input, resulting in increased submarine melt at the front (Liu *et al.* 2022); or (ii) surface-level ocean forcing resulting in a loss of winter rigid mélange, leading to increased calving (Bevan *et al.* 2019). Once again, understanding controls on tidewater glacier vulnerability is necessary for both identifying the climate and ocean conditions that lead to past retreat and for predicting future change.

Here, we examine recent changes at K.I.V Steenstrups Nordre Bræ (66.53 ˚N, 34.57 ˚W; fig. 1a; hereafter Steenstrup), an outlet glacier of the southeast Greenland Ice Sheet that exhibited long-term stability until a large destabilisation in 2018. We use observations and reanalysis products to outline the extent of change and understand the underlying mechanisms, identifying the sensitivities of the glacier to forcing out and outlining how this sensitivity changes through time.

2. Results

2.1. Temporal changes at Steenstrup

Prior to 2018, Steenstrup's calving front had been stable for decades, with an average 2015 front position only ~200 metres from the average 1985 front position (fig. 2a). The average speed at the calving front was ~7 m d^{-1} (~2.5 km a^{-1}) (fig. 1a), with an ice discharge of 3.34 Gt a^{-1} in 2016, putting it in the 82nd percentile of glaciers by contribution to Greenland's ice discharge (King *et al.*

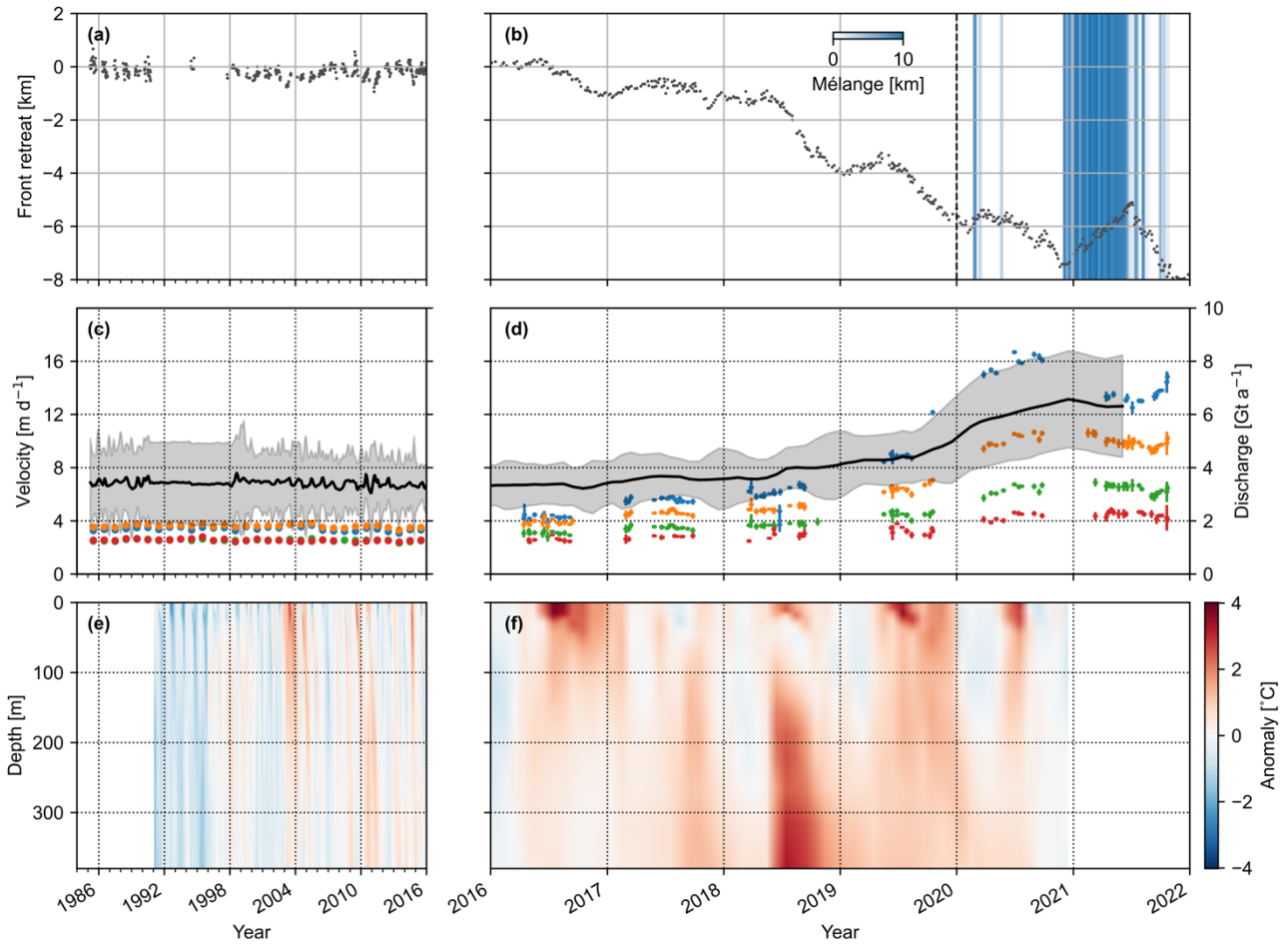

Figure 2: *Front position between (a) 1985 and 2015 and (b) 2016 and 2022, with blue shading denoting the the along-fjord extent of the rigid mélange measured from the glacier terminus between 2020 and 2021 (a zoomed 2020-2021 version of panel (b) is shown as fig. S1). Black dashed line marks beginning of the mélange record (January 2020). Ice discharge (black curve with shading as 2σ uncertainty) and annual velocity (colored points with errorbars) between (c) 1985 and 2015 and (d) 2016 and 2022. Point colours refer to points in Fig 1a. Mean ocean temperature anomaly from CMEMS Arctic Ocean Physics Reanalysis monthly mean data for the CE1 sample zone (fig. S5) between (e) 1992 and 2015 and (f) 2016 and 2021. An expanded version of the 2020-2021 mélange data is included as figure S1, and an expanded version of panels a, c, and e as fig. S2.*

2020). Seasonal variability in front position was low, with a standard deviation of 155 m. In most years, the front exhibited a negligible seasonal advance or retreat, with only a few exceptions to this rule (2002, 2009, 2010, 2014, 2016), where ~0.8-1.0 km of retreat occurred. This temporary retreat generally began in June but recovered, often overwinter but always within ~2 years. For instance, between early June 2016 and the 16th January 2017, Steenstrup's calving front retreated by ~1.3 km, before recovering ~0.7 km between January and June 2017.

In contrast, 2018 saw more significant and sustained retreats. This began in mid-May, totalling ~3.2 km by the 12th January, when the annual winter advance began. This pattern repeated in 2019, retreating ~3km between mid-May and early February. After a relatively short advance period relative to 2018, an additional ~2.1 km of retreat occurred between early May and November, 2020. At this point, the front began advancing, far earlier than in previous years and lasting much longer, into July 2021. By 4th July 2021, the terminus had advanced to the annual

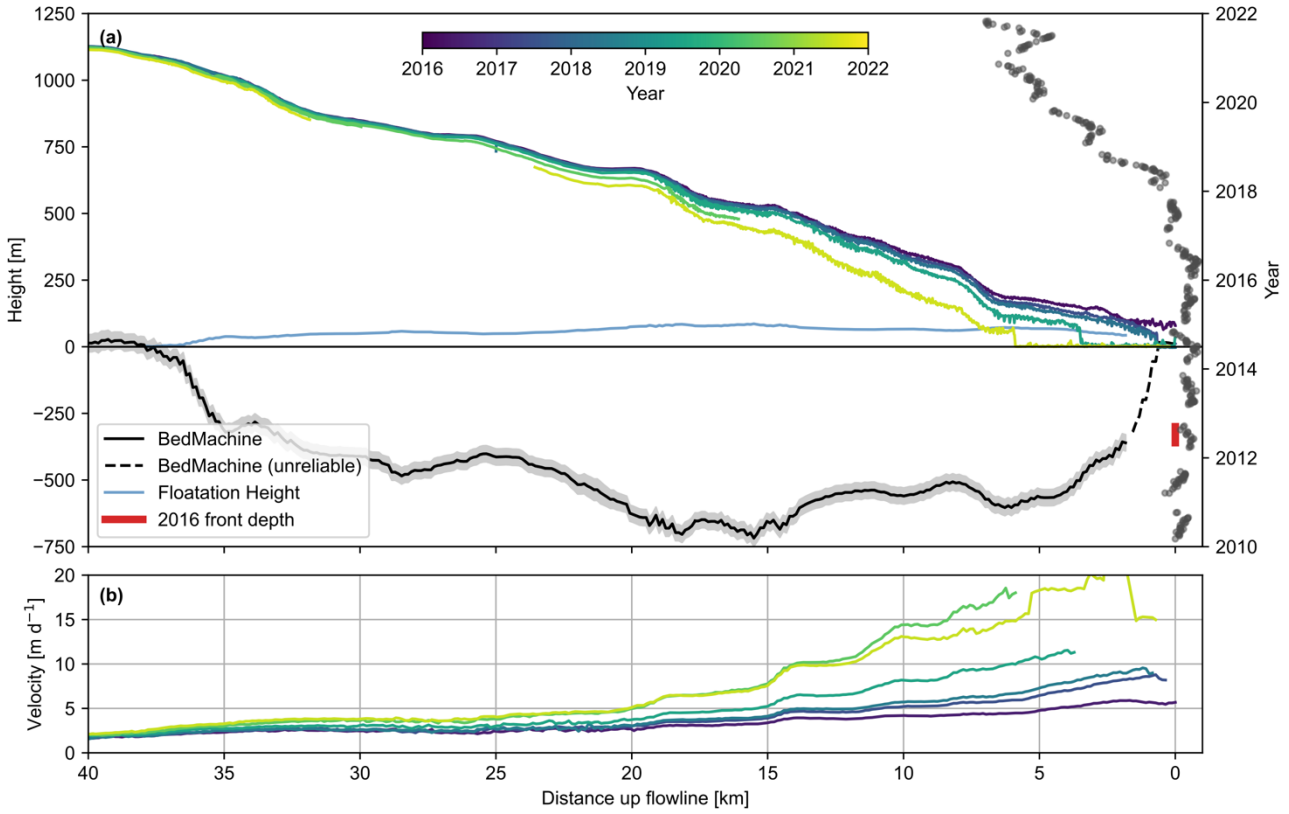

Figure 3: *(a) Surface (ArcticDEM strips) and bed elevation (BedMachine v4) along the profile shown in Fig. 1a. Blue line shows the floatation height of the ice column. Grey dots mark terminus positions through time. Red bar marks the vertical range of the 2016 terminus depth from Oceans Melting Greenland Multi Beam Echo Sounder data (Oceans Melting Greenland, 2019). Note that the front 1.8 km of the BedMachine data, denoted with a dashed line, is determined to be unreliable based on OMG and Operation IceBridge data (see supplementary text). (b) Annual speed profiles from ITS_LIVE velocity data along the profile shown in Fig. 1a.*

maxima, ~2.4 km from the November minima, and only ~0.3 km beyond the 2020 maxima. This advance was matched by a significant late-summer retreat of 2.9 km by early December, ultimately losing ~0.5 km relative to the annual minima of the previous year. In total, Steenstrup retreated ~7.1 km between 2018 and 2021.

Steenstrup's retreat occurred alongside an associated increase in glacier speed. After exhibiting no change between 1985-2016 (Fig 2b-c), speed increased at all sample points between 2016-2020. The frontmost sampling point reached a maximum of 16.8 m d^{-1} in August 2020 (an increase of more than 270%). However, alongside the front advance between November 2020 and July 2021, Steenstrup's speed greatly reduced, declining to ~12.8 m d^{-1} at the frontmost point by early July. At the point closest to the glacier front, acceleration occurred coincident with the retreat of the glacier calving front and continued for the rest of the year, reaching a maximum of 15.0 m d^{-1} in the last observation of the year (2021-10-22). However, it took time for this acceleration to propagate inland, with the two points further inland not accelerating until late August / early September, whilst the point furthest from the terminus showed no clear late-season acceleration. The total increased flow speed resulted in a doubling in the rate of ice discharge by 2021, reaching 6.37 Gt a^{-1} and placing Steenstrup in the 93rd percentile of Greenland's outlet

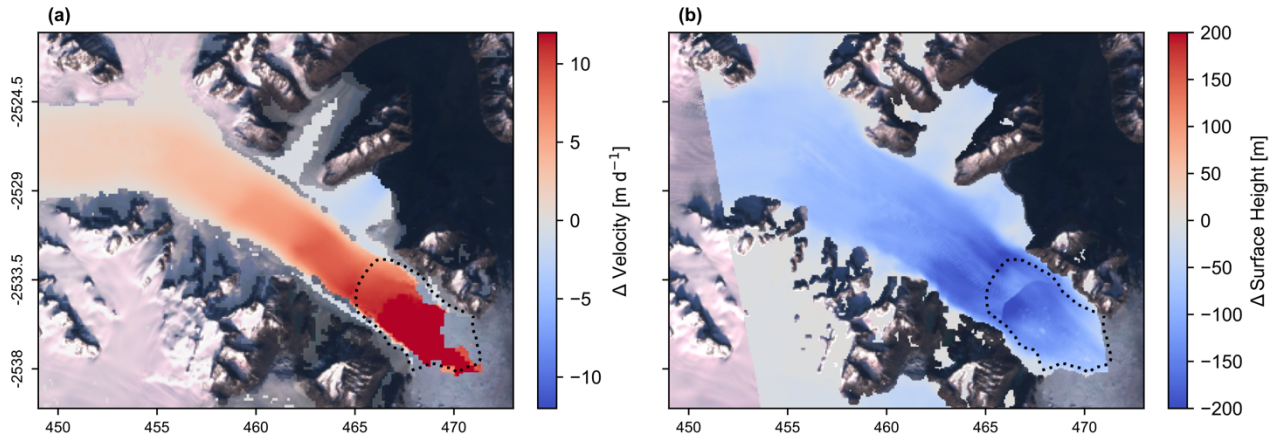

Figure 4: *Spatial extent of change. (a) Difference between the weighted mean average of 2021 and 2016 ITS_LIVE velocity pairs. Colours are translucent where change is not significant. (b) DEM difference between ArcticDEM strips captured on 2016-03-27 and 2021-07-31. Dotted lines mark terminus positions on 2016-09-28 and 2021-10-29. Coordinates in unit kilometres of NSIDC Polar Stereographic North.*

glaciers by contribution to total ice discharge, up from 3.34 Gt a^{-1} and 82nd percentile in 2016 (King *et al.* 2020).

Sampling annual velocity mosaics along the flowline (fig 3b) provides further information about the spatial extent of speed increases. Statistically significant increases in speed between 2016 and 2021 are visible up to 40 km inland, where speed increased 24% from 1.7 m d^{-1} in 2016 to 2.1 m d^{-1} in 2021. On average, speed increased over 100% within 19 km of the 2016 front position, over 50% within 27 km, and over 20% within 40 km. This acceleration was limited to the main glacier trunk: both distributaries exhibited statistically significant slowdowns, the northernmost distributary from ~0.5 m d^{-1} to ~0.2 m d^{-1}, and the southernmost from ~4.4 m d^{-1} to ~0.9 m d^{1} (fig. 4a). This contrasting behaviour between the main outlet and distributaries was associated with a significant shift in the medial moraine of the northernmost distributary as flow was captured by the main outlet (fig. S3).

Steenstrup's retreat was also associated with a significant reduction in surface elevation. Between 2016 and 2018, the surface of Steenstrup lowered by ~10 - 20 m a^{-1} within ~6 km of the 2016 front, with the rate of lowering decreasing to 1-2 m a^{-1} by 20 km inland (fig. 3a). However, after 2018, surface lowering accelerated and propagated inland rapidly. Between 8 and 10 km upglacier of the 2016 terminus, losses approached 50 m a^{-1} between 2018 and 2021. The Regional Atmospheric Climate Model (RACMO2.3p2) surface melt product (Noël *et al.* 2019) models maximum annual melt at Steenstrup for 2018-2021 period between 5.0 and 7.6 m a^{-1}, suggesting surface elevation change is far greater than could be attributed to increased surface melting and hence likely related to ice thinning under increased along-flow strain rates (i.e. dynamic thinning). By 2021, a combination of surface elevation loss and retreat along a retrograde bedslope resulted in ~1 km of the tongue being at or near flotation by 2021, as indicated by the ice surface height relative to flotation (fig. 3a). Total elevation losses exceeded 200 m between 2016 and 2020 (fig. 4b). Surface losses also occurred in the distributaries between 2016–2021: up to 40 m at the terminus of the northern distributary and 60 m at the southern distributary.

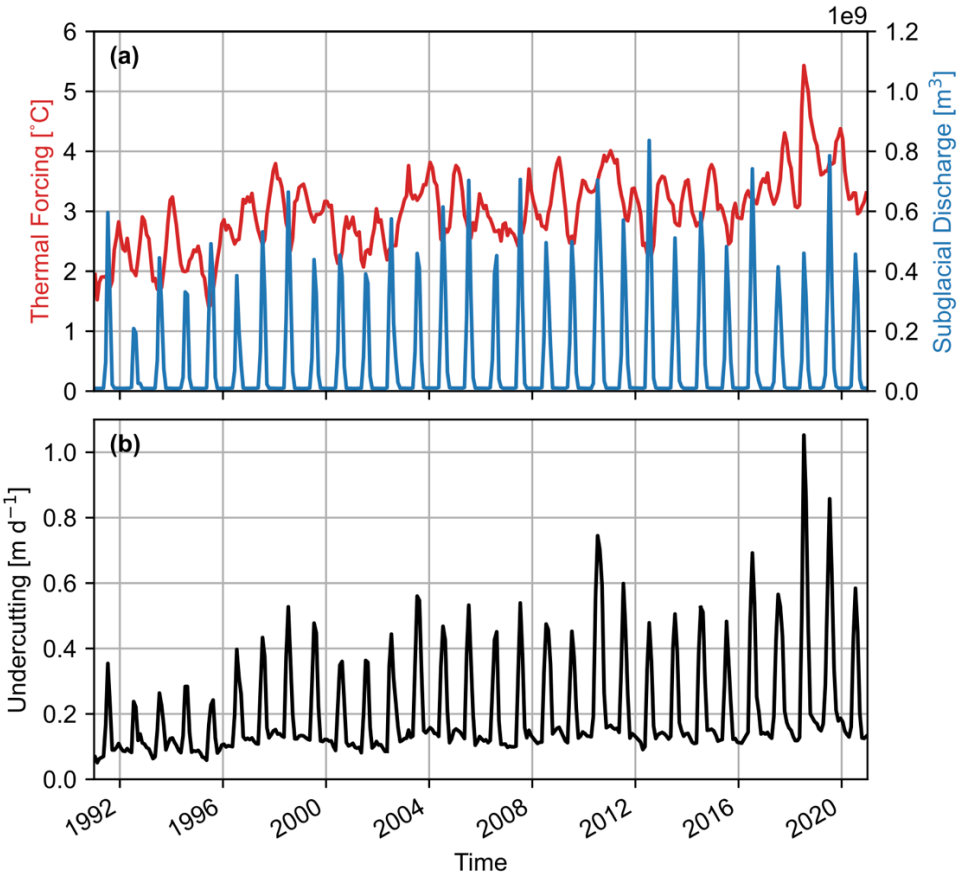

Figure 5: *Undercutting melt rate modelling results. (a) Time-varying inputs to thermal forcing parameterisation: the depth-averaged ocean thermal forcing in the lower 60% of the water column (red line) and the integrated monthly subglacial discharge of Steenstrup's hydrologic basin (blue line). (b) Modelled monthly average undercutting melt rate across the submerged calving face, in m* d^{-1}.

2.2. Forcing

Copernicus Marine Environment Monitoring Service (CMEMS) Arctic Ocean Physics Reanalysis monthly mean data (Copernicus Marine Environment Monitoring Service, 2021) (fig. 2e-f) indicate that positive anomalies in surface waters (relative to the 1992-2020 monthly mean) occurred frequently from ~2000 onwards, coincident with positive anomalies in estimates of subglacial discharge volumes from the RACMO2.3p2 surface melt product (fig. 5a). These increases were typically associated with seasonal retreats in front position (e.g., 2003, 2009, 2010, 2014, and 2016). In these cases, retreat was ephemeral and readvanced over the subsequent winter.

The significant retreat period that began in 2018 was synchronous with an exceptionally warm and thick temperature anomaly that is unprecedented since the start of the record and reached to within 100 m below the sea surface. At the deepest reanalysis level (380 m), this anomaly reached a maximum of +3.3 ˚C in July 2018 (the second-highest annual maxima, in October 2017, was only +1.3 ˚C). At 186 m (the reanalysis depth above which water could overtop the proglacial sill), the July 2018 anomaly was +2.4 ˚C. In contrast, the 2018 event did not coincide with large positive anomalies in surface water temperature (fig. 2f) or subglacial discharge driven by surface melt (fig. 5a).

Modelled undercutting melt rate peaked at an all-time high in July 2018 at 1.05 m d^{-1} (fig. 5b), with second-highest every peak levels following in July 2019 at 0.86 m d^{-1}. Supporting our above inferences, the 2018 record was driven by the record high in ocean thermal forcing rather than rates of subglacial discharge, which in 2018 was at only 86% of the long-term average annual high (fig. 5a). Historic anomalous undercutting rates in 2003, 2010, and 2016 align with temporary retreats in terminus front position, and appear to be driven by a combination of thermal forcing (e.g. 2003) and subglacial discharge (e.g. 2016).

3. Discussion

3.1. Rate and extent of destabilisation

Both this study and others indicate that Steenstrup has been stable on at least a decadal time scale prior to 2018. Data from the Landsat record (fig. 2a-b) is indicative of stability with very little seasonal variation going back to at least the 1980s. The front position further remains broadly the same in 1966 declassified satellite imagery (Cooper *et al.,* 2022) and 1938-1942 cartographic records (US Army Map Service, 1952), and a push moraine is present only 200 m from the 2016 front position (fig. S4a), which Batchelor *et al.* (2019) attribute to a 20th-century regime. Any significant advance beyond this was likely limited by a subsequent increase in exposed calving face to the ocean, whilst any retreat was stabilised by the front position on a ridge (e.g. Morlhigem *et al.* 2016, Millan *et al.* 2018).

The destabilisation that occurred between 2018-2021 was considerable in magnitude and extent. There was no significant precursor activity before the destabilisation, suggesting a sudden, external forcing. Steenstrup retreated ~7 km, thinned at nearly 50 m a^{-1}, quadrupled in speed, and doubled in ice discharge. Whilst retreat rates greater than 1000 m a^{-1} have precedent across tidewater glaciers (e.g. Hill *et al.* 2018), this retreat rate is still among the largest observed, with most glaciers retreating < 200 m a^{-1} (Bunce *et al.* 2018). Meanwhile, the dynamic thinning rate exceeds many significant glacier retreats, such as Kangerlussuaq (Kherl *et al.* 2017, Brough *et al.* 2019), and matches that of Sermeq Kujalleq during the early 2000s (Howat *et al.* 2007, Holland *et al.* 2008, Khazendar *et al.* 2019). Although absolute velocities are still lower, the quadrupling in speed within five years is, to our knowledge, unprecedented among the relative accelerations of large Greenland glaciers (Moon *et al.* 2012). This includes the approximate doubling in velocity over five years of Sermeq Kujalleq in the early 2000s (Howat *et al.* 2007). The short-term doubling of ice discharge is likewise unprecedented and only exceeded by Harald Moltke Bræ, which ~tripled its annual ice discharge within the span of a decade (King et al. 2020). However, this is explained by the glacier entering a surge phase, rather than as a response to external forcing (Müller *et al.* 2021). Hence, recent events at Steenstrup are comparable to, or exceed, the largest instances of tidewater glacier change across the Greenland Ice Sheet. Moon *et al.* (2012) suggested that rapid and large destabilisation may be limited to only a few glaciers. The case of Steenstrup, however, suggests that other, apparently stable, glaciers may still be primed to retreat under ever more positive forcing (Christian *et al.* 2022).

3.2. Forcing mechanisms

Prior studies have attributed post-2016 retreat of Greenland's south-eastern sector tidewater glaciers to two mechanisms. First, Bevan et al. (2019) attributed Kangerlussuaq's retreat to warm surface waters that prohibited the development of a rigid mélange in the winters of 2016/17 and 2017/18, leading to a loss of back stress and a subsequent increase in ice discharge, a mechanism supported with numerical modelling by Barnett *et al.* (2022). Second, in a broader sector-scale study, Liu et al. (2022) identified atmospheric forcing as the primary cause, with summers of high cumulative meltwater driving terminus melt via higher rates of subglacial discharge (e.g. Fried et al., 2018; Slater and Straneo 2022). However, both of these anomalous climate events, as well as accelerated glacier retreat across the sector, initiated in 2016. Although Steenstrup saw a seasonal retreat in 2016, it was commensurate with its historical response to other years with warm near-surface temperatures, including 2002, 2009, 2010, and 2014 (fig. 2a-b; fig. S2). Its 2017 advance indicates that Steenstrup was on a trajectory to recover its front position in line with previous seasonal retreats. Hence, Steenstrup did not share the extreme retreat response to surface temperature anomalies that was observed across the sector, even though relatively shallow, well-grounded glaciers such as Steenstrup have been hypothesised to be vulnerable to such events (e.g. Fried et al. 2018).

Insensitivity to mélange-destabilising events is consistent with the historical lack of mélange at Steenstrup. The optical satellite and ITS_LIVE velocity record shows that, prior to 2018, a small amount of mélange (on the order hundreds of metres) was observed in a small embayment on the southwest side of the terminus only. The reason behind an insensitivity to enhanced subglacial discharge remains less obvious. Liu et al. (2022) found no significant difference in runoff anomaly between glaciers that retreated in 2016 and those that did not, suggesting that high runoff alone is not sufficient alone to induce retreat. We suggest that the geometry of Steenstrup, with a confined and narrow trunk tens of kilometres long and ~100 km from the ice sheet proper, reduces the catchment area for surface melt runoff and increases subglacial transport times to the terminus. This consequently limits the rate and magnitude of subglacial meltwater discharge from the terminus, and hence the ability for surface melt to induce terminus melt. Additionally, the two distributaries near the front may provide alternative outlets for subglacially routed meltwater. In either case, these mechanisms are insufficient to explain Steenstrup's retreat.

Unstable retreat of Steenstrup began in 2018, with rates reaching kilometres per year between 2018 and 2021. This occurred alongside anomalously warm waters beneath ~100 m but no anomaly in near-surface temperatures (fig 2b; 5a), suggesting that Steenstrup's retreat was primarily initiated by submarine undercutting forced by warm AW (Seale et al. 2011, Straneo and Heinbach, 2013, Slater et al. 2020, An *et al.* 2018). This hypothesis is supported by our modelling results, which indicate that all-time highs in undercutting melt rates of 1.05 m d^{-1} were associated with AW thermal forcing and not subglacial discharge from surface melt (fig. 5a cf. 5b). In the high surface melt year of 2016, peak undercutting was 34% lower (0.69 m d^{-1}). The vulnerability of Steenstrup, which was relatively shallow and well-grounded at the ice front, to AW rather than mélange destabilisation or surface melt contrasts with expectations that AW is least effective at initiating retreat in shallow, well-grounded glaciers (Fried et al. 2018, Wood et al. 2021). Indeed, Wood et al. (2021) identify Steenstrup as a stable 'calving ridge' glacier, raised above the level of AW by a sill and having only a small floating section. It is of note, however, that this interpretation may be skewed by the poor topographic reconstruction of the terminus and near-terminus region

(see supplementary text). Oceans Melting Greenland Multi Beam Echo Sounder (OMG MBES) observations (Oceans Melting Greenland, 2019) a calving front depth in the range ~300-360 m and the lower limit of the proglacial sill at ~180 m (fig S4a). AW along the East Greenland Shelf primarily occurs beneath depths of ~250 m (Sutherland *et al.* 2013), above which cold and fresh polar water dominates. However, warm modes exist whereby AW can be present throughout the water column (Sutherland *et al.* 2013) and driven onto the coastal shelf (Jackson *et al.* 2014, Håvik and Våge, 2018). We suggest that 2018 is representative of an excessively warm mode (also identified in observational data by Snow *et al.* 2021) incorporating an anomalous amount of AW high into the water column at Kangerlussuaq Fjord (Fig. S6), which was then carried south across the coastal shelf as part of the East Greenland Coastal Current (Sutherland and Pickart, 2008; Håvik and Våge, 2018). The resultant anomaly in 2018 ocean temperatures extended to ~100 m in depth (fig 2b), far exceeding the ~180 m sill depth at Steenstrup. This is likely the first time that significant AW had been transported to the front of Steenstrup in the reanalysis record. AW presence across the shallow coastal shelf in front of Steenstrup (maximum depths of ~400 m) is rare compared to the front of Sermerlik and Kangerlussuaq Fjords, which have deep canyons to aid AW transfer (Sutherland *et al.* 2013; fig. S5). This is evident when comparing temperature anomaly data between the sites (figs. S5, S6). Although the warm 2018 anomaly is present at all locations, only in front of Steenstrup is it unprecedented within the record (fig. S6), suggesting that in 2018, AW could access even the shallowest sections of the coastal shelf. Increasing warming of waters around Greenland since the mid-1990s (Straneo and Heinbach, 2013) may result in increasingly common AW access to marine-terminating glaciers thought to be protected by shallow shelves and sills. However, predicting which are vulnerable may be challenging due to the poor knowledge of bed topography and proglacial bathymetry at many of the lesser-studied glaciers in Greenland.

3.3. Transition to mélange-dominated regime

Following destabilisation from the sill, Steenstrup retreated rapidly (~2 km a^{-1}) between 2018 and 2020 down a retrograde bedslope (fig 3a) until the front reached a second sill and stabilised in 2021. Following this retreat, Steenstrup began displaying a high seasonal variability in terminus position, advancing significantly in the 2020/21 winter before retreating in summer 2021. This advance/retreat pattern approximates the 'type b' glacier terminus behaviour described by Fried et al. (2018), retreating between ~June-September and advancing between ~September-June, which is attributed to the seasonal formation and breakup of mélange. This interpretation is supported by the mélange extent data (fig. 2b), which indicates that mélange was extensive in the 2020/21 winter but absent in 2019/20, and further supported by annual velocity mosaics, which record fast-flowing (>16 m d^{-1}) mélange in the 2021 mosaic but not between 1985 and 2020 (years 2016-2021 visualised in fig 3c). We suggest that by the 2020/21 winter, the retreat of the terminus ~6 km from fjord edge enabled mélange to form fast to the fjord margins, inducing backstress on the glacier front and suppressing calving rate (e.g. Todd and Christoffersen, 2014). This was aided by the glacier thinning sufficiently that the terminus 1 km from the front was at or near floatation (Amundson *et al.* 2010; fig. 3a), as well the fact that mélange buttressing has been shown to increase with the length-to-width ratio of the fjord (Schlemm and Levermann, 2021; Burton *et al.* 2018). These factors combined meant that the balance of stresses acting on the glacier terminus were more sensitive to the increased mélange backstress in the absence of reduced basal traction, modulating the new seasonal dynamic behaviour that emerged in 2021.

3.4. Steenstrup's future

Steenstrup's reatreat halted in 2021, likely due to a combination of reaching a section of prograde bedslope (fig 3a), a reduction in driving stress due to rapid dynamic thinning, and the development of a rigid proglacial mélange. However, the glacier is by no means stable. With velocities quadrupled since 2016, Steenstrup is likely far out of balance. Ice flow is confined to relatively narrow valleys and catchments until connecting to the ice sheet over 100 km upstream, limiting influx (fig. 1a). As such, diffusive acceleration is concentrated in the trunk, increasing rates of dynamic thinning relative to less confined glaciers (Moon et al. 2012). In this sense, the upstream response to retreat is similar to Alaskan tidewater glaciers, such as Columbia Glacier (Walter *et al.* 2010). Rapid thinning is resolvable tens of kilometres inland (fig. 3a) and this imbalance in ice discharge will likely persist due to a transition to a deeper terminus that is at or near floatation (fig. 3a). This has been suggested to enhance tabular calving driven by full-thickness fracture (Carr *et al.* 2013, Fried et al. 2018) rather than smaller, sub-aerial calving events, a transition reported at Columbia (Walter *et al.* 2010) and Bowdoin Glaciers (van Dongen *et al.* 2021). We hypothesise that these factors make the 2021 terminus position untenable in the medium term, even accounting for the current position on a bedrock bump (fig. 3a).

The next ~8 km of retreat will be influenced by the collapse of the two tidewater distributaries, which are already thinning rapidly (fig. 4b). As these areas are also decelerating (fig. 4a), we suggest that this is not due to dynamic thinning but instead due to decreasing influx resulting from flow capture by the main trunk (fig. S3). Once the main terminus retreats past the distributaries, they will rapidly disintegrate due to submarine melt and calving. However, their collapse will once again restrict the ability of a rigid mélange to form by reducing the length-to-width ratio of the fjord area available (Schlemm and Levermann, 2021; Burton *et al.* 2018) due to a lack of fjord margins on the northeast side. This will enhance calving rates of the main trunk (Schlemm and Levermann, 2021) and further enable retreat. Understanding of the basal topography is poor in this sector (see supplementary text), but visual analysis of airborne radar data (fig. S7) suggests that retrograde bedslopes likely continue to occur, with some rises that may or may not stall retreat (Robel *et al.* 2022), until approximately 20 km from the 2016 calving front. The extent to which the glacier stabilises or not between this point and when the bed reaches sea level (35 km inland) will be controlled by the full extent of dynamic thinning and ocean forcing.

Retrograde bed slopes above the current front position, imminent destabilisation, loss of distributaries, and continued dynamic thinning all indicate further, rapid retreat of Steenstrup. However, the relative influence of atmospheric and oceanic forcing may modify the rate of response, especially at prograde bedrock rises. As identified above, Steenstrup's seasonal behaviour in 2021 suggests a new sensitivity to mélange variability. As a result, Steenstrup may now be newly vulnerable to ocean surface temperature, as occurred in 2016 at Kangerlussuaq (Bevan *et al.* 2019; Barnett *et al.* 2022). Meanwhile, sensitivity to warm AW instrusions will continue, especially if the collapse of the two northeastern distributaries provide new pathways for AW entry through the deeper northern fjord (fig. S4b). The future sensitivity of the glacier to surface melt and resultant subglacial discharge is less clear. However, a quadrupling in velocity may result in an increase in subglacial melt generated via frictional heating at the bed, whilst the increased positive surface strain rates in accelerating zones may provide new pathways for water

to reach the bed through crevasses. As a result, the changes occurring at Steenstrup may make it more vulnerable to a range of tidewater glacier retreat mechanisms.

4. Implications

Steenstrup provides a unique example of rapid glacier change that has occurred entirely within a period of intense observational study from various Earth observation instruments. Occurring without resolvable precursor activity, the destabilisation of Steenstrup from 2018 onwards marks one of the most significant rapid responses of a tidewater glacier, particularly from a glacier previously thought to be stable and insensitive to ocean forcing. The various responses to forcing exhibited between 2016 and 2021 prove instructive in verifying theories of ice-ocean sensitivity and highlight the ability of a tidewater glacier to transition between sensitivity to warm AW and warm surface temperatures (via mélange), whilst remaining broadly insensitive to enhanced surface melt. Relative to retreats of other major outlet glaciers like Sermeq Kujalleq and Kangerdlugssuaq, thinning and acceleration propagating inland from the ice front were amplified by Steenstrup's more confined geometry. Already possibly the highest relative increase in glacier speed observed amongst fast-moving tidewater glaciers in Greenland, significant change can be expected to continue into the coming years and decades. This makes Steenstrup a priority for ongoing observation as well as a good candidate for numerical modelling experiments: providing both the opportunity to test the ability of models to replicate complex changes and forcings, and to provide future projections that will be falsifiable on a timescale of years.

Model reanalysis presented here and elsewhere (e.g. Wood *et al.* 2021) show that AW around the GrIS is becoming progressively warmer in recent decades (Straneo and Heinbach, 2013), providing increasing opportunities for warm waters to penetrate to the front of marine-terminating glaciers that are relatively more protected from incursions by proglacial bathymetry (Christian *et al.* 2022). Steenstrup has shown that the stability of glaciers is hard to predict using our current knowledge of smaller, stable, and data-sparse glaciers, especially given the apparently poor reconstruction of the geometry of the ice-ocean interface at Steenstrup and elsewhere. There may be many more well-grounded and mélange-deficient glaciers that, whilst resistant to warm surface waters and subglacial discharge, are primed to retreat and increase their contribution to total GrIS ice discharge in the face of increasing AW incursion.

5. Methods

5.1. Calving front positions

Calving front positions were manually digitised along the centreline between 1985 and 2021 using Landsat 4 - 8, ASTER, and Sentinel-1 data following Walsh *et al.* (2012).

5.2. Glacier velocity

We investigated the change in speed of Steenstrup with both scene-pair velocities (to construct time-series) and annual velocity maps (to assess spatial change). To do this, we make use of ITS_LIVE velocity data (Gardner et al., 2018, 2021). Between 1985 and 2015, we downloaded annual mosaics of velocity provided by the ITS_LIVE project (Fig. 2c). Beyond 2016 (Fig. 2b), we

download all available scene-pair velocity data covering Steenstrup between 2016 and 2021 with >1% data coverage.

To present a time series (Fig. 2b) ITS_LIVE velocity pairs were sampled at locations between 6 km and 23 km along the flowline from the 2016 calving front (Table S1). We use 2016 as our pre-retreat standard across all observed variables as in 2017 the glacier was recovering from a minor retreat forced in late 2016 (section 2.1), displayed a retreated terminus and slightly enhanced velocity relative to 1985-2016 norm (fig. 2). We sample a 1 km × 1 km box centred on the point, presenting the median speed and error of the sample zone where coverage is greater than 70%.

As updated annual mosaics between 2019-2021 were not available at the time of writing, we calculated our own annual mosaics to produce difference maps between 2016 and 2021 for visualisation (Fig. 3b, 4a). From the provided speed (x) and error (σ) values, we calculate the weighted mean ($\bar{x}$) as:

$$\bar{x} = \frac{\sum x/\sigma^2}{\sum 1/\sigma^2}$$

and the weighted standard error ($\bar{\sigma}$) as:

$$\bar{\sigma} = \frac{1}{\sum 1/\sigma^2}$$

A two-tailed unpaired *t*-test is used to assess whether differences between the mosaic pixels are significant (Fig. 4a).

5.3. Mélange presence

Mélange velocities were derived for continuous 6-day periods throughout 2020 and 2021 from SAR imagery acquired in the interferometric wide swath (IW) mode from the Sentinel-1 A and B. Velocity maps over rigid mélange-occupied regions of the fjord and surrounding margin were processed following GrIMP workflows (Joughin *et al.* 2021), which measure 6-day displacements of features in image pairs by cross-correlating small (km-scale) image patches using a combination of speckle and feature tracking of the textured mélange surface. Here, we measure only the extent of rigid mélange, or regions of icebergs and sea ice that can be tracked from one image to the next because they maintain coherence, using the intersection of the rigid melange patch with an extended center flowline (fig. X?). By contrast, the mapping algorithm fails if the mélange is non-rigid, or such that the individual constituents of the mélange move more randomly relative to each other. Based on this principle, we did not process prior to 2020, as no rigid mélange signature were present in any ITS_LIVE mosaics between 1985 and 2020. When present, the extent of rigid mélange is derived by comparing the distance between the outer limit of rigid mélange areas, to the contemporaneous Steenstrup terminus position, which is manually traced at the same 6-day temporal resolution. Thus, in addition to understanding whether or not rigid mélange is present adjacent to the terminus at a given time step, mélange extent provides a metric to evaluate potential relative back force at the calving front.

5.4. Ice Discharge

Monthly ice discharge from 1985 through 2021 was calculated through an upstream flux gate (fig. 1), oriented perpendicular to ice flow, across the width of Steenstrup. Following methods outlined

in King *et al*. (2018, 2020), we sample ice thicknesses and ice velocities at points every 250 m along this gate. As in King et al. (2020), velocities were obtained from both optical and SAR data, with time series appended through 2021 using velocities from GrIMP Sentinel 1A & 1B (Joughin, 2022). Temporal data gaps are filled using a Kalman filter approach as described in King et al. (2018), and the final time series of combined velocities are smoothed using a moving filter weighted by observational errors, which arise due to noise-to-pixel ratios and co-registration quality between paired images. Ice thicknesses were obtained from differencing surface elevations from historic DEM data (ranging from AeroDEM through Arctic DEM) with bathymetry from BedMachine v4. Total ice thickness errors include the combined spatially variable and systematic errors from the BedMachine product with an estimated random error of 5 m from surface elevation data. Monthly ice discharge estimates were calculated by summing the product of ice thickness, velocity, and ice density (910 kg m^{-3}) at each 250 m along-gate bin (fig. S8). Continuous uncertainty bounds reflect the standard deviation of a 1000-iteration Monte Carlo ensemble that perturbs the time series with random errors within each time step's error bounds. applied to the time series with random errors applied at each time step.

5.5. Topographic Analysis

To assess elevation change over the period of interest, we use 2 m ArcticDEM strips (Porter *et al.* 2018). From the archive, we manually identify high-quality strips between 2016–2012 (Table S2), coregistering the strips to the 2016 DEM following the method of Nuth and Kääb (2011).

To explore the potential for floatation at the calving front, we estimate the theoretical floatation thickness (H_f) based on basal topography extracted from BedMachine v4 (Morlighem *et al.* 2017; Morlighem *et al.* 2021) as

$$H_f = -h_b \frac{\rho_w}{\rho_i}$$

where H_b is the bed depth, and ρ_i and ρ_w , are the densities of ice and water (assigned 917 and 1027 kg m^{-3}) respectively.

5.6. Oceanography data

5.6.1. Temperature Data

Following Bevan *et al.* (2021), we extract ocean potential temperatures from 1991-2020 from the Copernicus Marine Environment Monitoring Service (CMEMS) Arctic Ocean Physics Reanalysis monthly mean data (Copernicus Marine Environment Monitoring Service, 2021). We convert potential temperatures to thermal forcing (the difference between the in-situ temperature and freezing point of seawater), using pressure and salinity to calculate the freezing point as

$$t_f = a_0 S + a_1 S^{3/2} + a_2 S^2 + bp$$

where t_f is the freezing point temperature, S is salinity, p is pressure, and the remainder are constants (a_0 = -0.0575, a_1 = 1.710523e^{-3}, a_2 = -2.154996e^{-4}, and b = -7.52e^{-4}) following Fofonoff and Millard Jr (1983). We calculated monthly anomalies in the thermal forcing over the continental shelf in front of KJV Steenstrup (fig. 2b). Here, we use sampling zones matching Wood *et al.* (2021) – specifically zone CE1 (fig. S5).

5.6.2. Bathymetry

Bathymetric data (fig. S4,5) is derived regionally from the International Bathymetric Chart of the Arctic Ocean (IBCAO) Grid v4.1 (Jakobson *et al.* 2020), and locally from multi-beam echo sounding (MBES) bathymetry data from the Oceans Melting Greenland (OMG) project (OMG, 2019).

5.6.3. Undercut Modelling

Following Rignot *et al.* (2016) and Wood *et al.* (2021), the rate of undercutting (monthly average melt rate across the submerged calving face) is parameterised as

$$q_m = \left(A \;\; h \;\; q_{sg}^{\alpha} \;\; B\right) TF^{\beta}$$

h is the average water depth across the calving front, set at 320 m based on OMG MBES data. TF is the depth-averaged monthly ocean thermal forcing in the lower 60% of the water column, from CMEMS data. q_{sg} is the basin-integrated monthly subglacial discharge averaged over the glacier front area (width 4000 m). The hydrological basin of Steenstrup is taken from Mankoff *et al*. (2020) with k=0.9, and the subglacial discharge represents the sum of (i) the basin-integrated monthly surface runoff is from RACMO2.3p2 at 1 km resolution, statistically downscaled from 5.5 km (Noël *et al.*, 2019); and (ii) basin-integrated monthly subglacial melt, assumed constant, from Karlsson *et al.* (2021). Constants A (3×10^4), α (0.39), B (0.15), and β (1.18) are set following Rignot *et al.* (2016). The output, q_m, is the average across the submerged calving face, in metres per day. The mean nominal uncertainty is assigned at 26%, following Rignot *et al.* (2016) and Wood *et al.* (2021).

Acknowledgements

This project was supported by grants 80NSSC18K1027 and NNX13AI21A from the National Aeronautics and Space Administration. We are grateful to Christine Batchelor for assistance with interpretation of bathymetric data, and to Mike Wood for supplying his sample zones and for discussions regarding undercutting parameterisation.

Author Contributions

TRC: Conceptualisation, Investigation, Formal analysis, Visualisation, Writing - Original Draft. IMH: Conceptualisation, Investigation, Resources, Funding acquisition, Project administration, Supervision, Writing - Review & Editing. MDK: Investigation, Writing - Review & Editing. AN: Investigation.

Data Availability

Data necessary to replicate this study and the figures within are available from Zenodo at https://doi.org/10.5281/zenodo.6903789 (Chudley *et al.* 2022). This includes terminus positions, ice discharge history, mélange data, custom ITS_LIVE annual velocity fields, ocean reanalysis data, and modelling inputs and results. ITS_LIVE scene-pair data are available from https://doi.org/10.5067/IMR9D3PEI28U (Gardner *et al.* 2022). ArcticDEM 2m strips are available at

https://doi.org/10.7910/DVN/OHHUKH (Porter *et al.* 2018). The CMEMS Arctic Ocean Physics Reanalysis monthly product is available from https://doi.org/10.48670/moi-00007. BedMachine v4 is available at https://doi.org/10.5067/VLJ5YXKCNGXO (Morlighem *et al.* 2021). IBCAO v4 is available from https://www.gebco.net/ (Jakobsson *et al.* 2020). OMG MBES gridded data is available from https://www.doi.org/10.5067/OMGEV-MBES1 (Oceans Melting Greenland, 2019). The monthly cumulative runoff product for Greenland from RACMO2.3p2 is freely available from the authors of Noël *et al.* (2019) upon request and without conditions.

Code Availability

Python code necessary to replicate the melt undercut modelling is included as a Jupyter Notebook alongside the data repository at https://doi.org/10.5281/zenodo.6903790 (Chudley *et al.* 2022).

References

Amundson, J. M., Fahnestock, M., Truffer, M., Brown, J., Lüthi, M. P., & Motyka, R. J. (2010). Ice mélange dynamics and implications for terminus stability, Jakobshavn Isbræ, Greenland. *Journal of Geophysical Research: Earth Surface*, *115*(F1). https://doi.org/10.1029/2009JF001405

An, L., Rignot, E., Wood, M., Willis, J. K., Mouginot, J., & Khan, S. A. (2021). Ocean melting of the Zachariae Isstrøm and Nioghalvfjerdsfjorden glaciers, northeast Greenland. Proceedings of the National Academy of Sciences, 118(2), e2015483118. https://doi.org/10.1073/pnas.2015483118

Army Map Service (1952). AMS C501 Greenland 1:250,000 Topographic Series - Sheet NQ 25, 26-5 'KJV Steenstrups Søndre Bræ'. Corps of Engineers, U.S. Army, Washington DC. Downloaded from the Polar Geospatial Center https://maps.apps.pgc.umn.edu/id/394

Barnett, J., Holmes, F. A., & Kirchner, N. (2022). Modelled dynamic retreat of Kangerlussuaq Glacier, East Greenland, strongly influenced by the consecutive absence of an ice mélange in Kangerlussuaq Fjord. *Journal of Glaciology*, 1–12. https://doi.org/10.1017/jog.2022.70

Batchelor, C. L., Dowdeswell, J. A., Rignot, E., & Millan, R. (2019). Submarine Moraines in Southeast Greenland Fjords Reveal Contrasting Outlet-Glacier Behavior since the Last Glacial Maximum. Geophysical Research Letters, 46(6), 3279–3286. https://doi.org/10.1029/2019GL082556

Bevan, S. L., Luckman, A. J., Benn, D. I., Cowton, T., & Todd, J. (2019). Impact of warming shelf waters on ice mélange and terminus retreat at a large SE Greenland glacier. The Cryosphere, 13(9), 2303–2315. https://doi.org/10.5194/tc-13-2303-2019

Bindschadler, R., Vornberger, P., Blankenship, D., Scambos, T., & Jacobel, R. (1996). Surface velocity and mass balance of Ice Streams D and E, West Antarctica. Journal of Glaciology, 42(142), 461–475. https://doi.org/10.3189/S0022143000003452

Brough, S., Carr, J. R., Ross, N., & Lea, J. M. (2019). Exceptional retreat of Kangerlussuaq Glacier, east Greenland, between 2016 and 2018. Frontiers in Earth Science, 7, 123. https://doi.org/10.3389/feart.2019.00123

Bunce, C., Carr, J. R., Nienow, P. W., Ross, N., & Killick, R. (2018). Ice front change of marine-terminating outlet glaciers in northwest and southeast Greenland during the 21st century. Journal of Glaciology, 64(246), 523–535. https://doi.org/10.1017/jog.2018.44

Burton, J. C., Amundson, J. M., Cassotto, R., Kuo, C.-C., & Dennin, M. (2018). Quantifying flow and stress in ice mélange, the world's largest granular material. Proceedings of the National Academy of Sciences, 115(20), 5105–5110. https://doi.org/10.1073/pnas.1715136115

Carr, J. R., Stokes, C., & Vieli, A. (2014). Recent retreat of major outlet glaciers on Novaya Zemlya, Russian Arctic, influenced by fjord geometry and sea-ice conditions. Journal of Glaciology, 60(219), 155–170. https://doi.org/10.3189/2014JoG13J122

Carr, J. R., Vieli, A., & Stokes, C. (2013). Influence of sea ice decline, atmospheric warming, and glacier width on marine-terminating outlet glacier behavior in northwest Greenland at seasonal to interannual timescales. Journal of Geophysical Research: Earth Surface, 118(3), 1210–1226. https://doi.org/10.1002/jgrf.20088

Cassotto, R., Fahnestock, M., Amundson, J. M., Truffer, M., & Joughin, I. (2015). Seasonal and interannual variations in ice melange and its impact on terminus stability, Jakobshavn Isbræ, Greenland. Journal of Glaciology, 61(225), 76–88. https://doi.org/10.3189/2015JoG13J235

Cassotto, R., Fahnestock, M., Amundson, J. M., Truffer, M., Boettcher, M. S., Peña, S. D. L., & Howat, I. (2019). Non-linear glacier response to calving events, Jakobshavn Isbræ, Greenland. Journal of Glaciology, 65(249), 39–54. https://doi.org/10.1017/jog.2018.90

Catania, G. A., Stearns, L. A., Moon, T. A., Enderlin, E. M., & Jackson, R. (2020). Future Evolution of Greenland's Marine-Terminating Outlet Glaciers. Journal of Geophysical Research: Earth Surface, 125(n/a), e2018JF004873. https://doi.org/10.1029/2018JF004873

Christian, J. E., Robel, A. A., & Catania, G. (2022). A probabilistic framework for quantifying the role of anthropogenic climate change in marine-terminating glacier retreats. The Cryosphere, 16(7), 2725–2743. https://doi.org/10.5194/tc-16-2725-2022

Chudley, T. R., Howat, I. M., King, M. D., & Negrete, A.. (2022). Data supporting 'Atlantic Water intrusion triggers sudden and rapid retreat of Greenlandic glacier following long-term stability'. Zenodo. https://doi.org/10.5281/zenodo.6903790

Cooper, M. A., Lewińska, P., Smith, W. A. P., Hancock, E. R., Dowdeswell, J. A., & Rippin, D. M. (2022). Unravelling the long-term, locally heterogenous response of Greenland glaciers observed in archival photography. The Cryosphere, 16(6), 2449–2470. https://doi.org/10.5194/tc-16-2449-2022

Copernicus Marine Environment Monitoring Service (2021), ARCTIC_MULTIYEAR_PHY_002_003, [dataset] https://doi.org/10.48670/moi-00007

van Dongen, E. C. H., Jouvet, G., Sugiyama, S., Podolskiy, E. A., Funk, M., Benn, D. I., et al. (2021). Thinning leads to calving-style changes at Bowdoin Glacier, Greenland. The Cryosphere, 15(2), 485–500. https://doi.org/10.5194/tc-15-485-2021

Enderlin, E. M., Howat, I. M., & Vieli, A. (2013). High sensitivity of tidewater outlet glacier dynamics to shape. The Cryosphere, 7(3), 1007–1015. https://doi.org/10.5194/tc-7-1007-2013

Enderlin, Ellyn M., & Bartholomaus, T. C. (2020). Sharp contrasts in observed and modeled crevasse patterns at Greenland's marine terminating glaciers. The Cryosphere, 14(11), 4121–4133. https://doi.org/10.5194/tc-14-4121-2020

Felikson, D., Bartholomaus, T. C., Catania, G. A., Korsgaard, N. J., Kjær, K. H., Morlighem, M., et al. (2017). Inland thinning on the Greenland ice sheet controlled by outlet glacier geometry. Nature Geoscience, 10(5), 366–369. https://doi.org/10.1038/ngeo2934

Fofonoff, N. P., & Millard Jr, R. C. (1983). Algorithms for the computation of fundamental properties of seawater. Paris, France, UNESCO, 53pp. (UNESCO Technical Papers in Marine Sciences; 44). https://doi.org/10.25607/OBP-1450

Fried, M. J., Catania, G. A., Bartholomaus, T. C., Duncan, D., Davis, M., Stearns, L. A., et al. (2015). Distributed subglacial discharge drives significant submarine melt at a Greenland tidewater glacier. Geophysical Research Letters, 42(21), 9328–9336. https://doi.org/10.1002/2015GL065806

Fried, M. J., Catania, G. A., Stearns, L. A., Sutherland, D. A., Bartholomaus, T. C., Shroyer, E., & Nash, J. (2018). Reconciling Drivers of Seasonal Terminus Advance and Retreat at 13 Central West Greenland Tidewater Glaciers. Journal of Geophysical Research: Earth Surface, 123(7), 1590–1607. https://doi.org/10.1029/2018JF004628

Gardner, A. S., Moholdt, G., Scambos, T., Fahnstock, M., Ligtenberg, S., van den Broeke, M., & Nilsson, J. (2018). Increased West Antarctic and unchanged East Antarctic ice discharge over the last 7 years. The Cryosphere, 12(2), 521–547. https://doi.org/10.5194/tc-12-521-2018

Gardner, A. S., M. A. Fahnestock, and T. A. Scambos. (2022). MEaSUREs ITS_LIVE Landsat Image-Pair Glacier and Ice Sheet Surface Velocities: Version 1, [dataset] https://doi.org/10.5067/IMR9D3PEI28U

Håvik, L., & Våge, K. (2018). Wind-Driven Coastal Upwelling and Downwelling in the Shelfbreak East Greenland Current. Journal of Geophysical Research: Oceans, 123(9), 6106–6115. https://doi.org/10.1029/2018JC014273

Hill, E. A., Carr, J. R., Stokes, C. R., & Gudmundsson, G. H. (2018). Dynamic changes in outlet glaciers in northern Greenland from 1948 to 2015. The Cryosphere, 12(10), 3243–3263. https://doi.org/10.5194/tc-12-3243-2018

Holland, D. M., Thomas, R. H., de Young, B., Ribergaard, M. H., & Lyberth, B. (2008). Acceleration of Jakobshavn Isbræ triggered by warm subsurface ocean waters. Nature Geoscience, 1(10), 659–664. https://doi.org/10.1038/ngeo316

Howat, I. M., Joughin, I., & Scambos, T. A. (2007). Rapid Changes in Ice Discharge from Greenland Outlet Glaciers. Science, 315(5818), 1559–1561. https://doi.org/10.1126/science.1138478

Jackson, R. H., Straneo, F., & Sutherland, D. A. (2014). Externally forced fluctuations in ocean temperature at Greenland glaciers in non-summer months. Nature Geoscience, 7(7), 503–508. https://doi.org/10.1038/ngeo2186

Jakobsson, M., Mayer, L. A., Nilsson, J., Stranne, C., Calder, B., O'Regan, M., et al. (2020). Ryder Glacier in northwest Greenland is shielded from warm Atlantic water by a bathymetric sill. Communications Earth & Environment, 1(1), 1–10. https://doi.org/10.1038/s43247-020-00043-0

Jakobsson, M., Mayer, L. A., Bringensparr, C., Castro, C. F., Mohammad, R., Johnson, P., et al. (2020). The International Bathymetric Chart of the Arctic Ocean Version 4.0. Scientific Data, 7(1), 176. https://doi.org/10.1038/s41597-020-0520-9

Jensen, C. D. (2022) Weather Observations from Greenland 1958-2021 – Observational Data with Description. DMI Report No. 22-08. https://www.dmi.dk/publikationer/

Joughin, I. (2022). MEaSUREs Greenland 6 and 12 day Ice Sheet Velocity Mosaics from SAR, Version 2. Boulder, Colorado USA. NASA National Snow and Ice Data Center Distributed Active Archive Center. https://doi.org/10.5067/1AMEDB6VJ1NZ. Date Accessed 10-17-2022.

Joughin, I., Shean, D. E., Smith, B. E., & Floricioiu, D. (2020). A decade of variability on Jakobshavn Isbræ: ocean temperatures pace speed through influence on mélange rigidity. The Cryosphere, 14(1), 211–227. https://doi.org/10.5194/tc-14-211-2020

Karlsson, N. B., Solgaard, A. M., Mankoff, K. D., Gillet-Chaulet, F., MacGregor, J. A., Box, J. E., et al. (2021). A first constraint on basal melt-water production of the Greenland ice sheet. Nature Communications, 12(1), 3461. https://doi.org/10.1038/s41467-021-23739-z

Kehrl, L. M., Joughin, I., Shean, D. E., Floricioiu, D., & Krieger, L. (2017). Seasonal and interannual variabilities in terminus position, glacier velocity, and surface elevation at Helheim and Kangerlussuaq Glaciers from 2008 to 2016. Journal of Geophysical Research: Earth Surface, 122(9), 1635–1652. https://doi.org/10.1002/2016JF004133

Khazendar, A., Fenty, I. G., Carroll, D., Gardner, A., Lee, C. M., Fukumori, I., et al. (2019). Interruption of two decades of Jakobshavn Isbrae acceleration and thinning as regional ocean cools. Nature Geoscience, 12(4), 277–283. https://doi.org/10.1038/s41561-019-0329-3

King, M. D., Howat, I. M., Jeong, S., Noh, M. J., Wouters, B., Noël, B., & van den Broeke, M. R. (2018). Seasonal to decadal variability in ice discharge from the Greenland Ice Sheet. *The Cryosphere*, *12*(12), 3813.

King, M. D., Howat, I. M., Candela, S. G., Noh, M. J., Jeong, S., Noël, B. P. Y., et al. (2020). Dynamic ice loss from the Greenland Ice Sheet driven by sustained glacier retreat. Communications Earth & Environment, 1(1), 1–7. https://doi.org/10.1038/s43247-020-0001-2

Lea, J. M. (2018). The Google Earth Engine Digitisation Tool (GEEDiT) and the Margin change Quantification Tool (MaQiT) – simple tools for the rapid mapping and quantification of changing Earth surface margins. Earth Surface Dynamics, 6(3), 551–561. https://doi.org/10.5194/esurf-6-551-2018

Liu, J., Enderlin, E., Marshall, H.-P., & Khalil, A. (2022). Synchronous retreat of southeast Greenland's peripheral glaciers. Geophysical Research Letters, n/a(n/a), e2022GL097756. https://doi.org/10.1029/2022GL097756

Mankoff, K. D., Noël, B., Fettweis, X., Ahlstrøm, A. P., Colgan, W., Kondo, K., Langley, K., Sugiyama, S., van As, D., and Fausto, R. S. (2020). Greenland liquid water discharge from 1958 through 2019, Earth Syst. Sci. Data, 12, 2811–2841, https://doi.org/10.5194/essd-12-2811-2020

McFadden, E. M., Howat, I. M., Joughin, I., Smith, B. E., & Ahn, Y. (2011). Changes in the dynamics of marine terminating outlet glaciers in west Greenland (2000–2009). Journal of Geophysical Research: Earth Surface, 116(F2). https://doi.org/10.1029/2010JF001757

Millan, R., Rignot, E., Mouginot, J., Wood, M., Bjørk, A. A., & Morlighem, M. (2018). Vulnerability of Southeast Greenland Glaciers to Warm Atlantic Water From Operation IceBridge and Ocean Melting Greenland Data. Geophysical Research Letters, 45(6), 2688–2696. https://doi.org/10.1002/2017GL076561

Moon, T., Joughin, I., & Smith, B. (2015). Seasonal to multiyear variability of glacier surface velocity, terminus position, and sea ice/ice mélange in northwest Greenland. Journal of Geophysical Research: Earth Surface, 120(5), 818–833. https://doi.org/10.1002/2015JF003494

Morlighem, M., Bondzio, J., Seroussi, H., Rignot, E., Larour, E., Humbert, A., & Rebuffi, S. (2016). Modeling of Store Gletscher's calving dynamics, West Greenland, in response to ocean thermal forcing. Geophysical Research Letters, 43(6), 2659–2666. https://doi.org/10.1002/2016GL067695

Morlighem, M., Williams, C. N., Rignot, E., An, L., Arndt, J. E., Bamber, J. L., et al. (2017). BedMachine v3: Complete Bed Topography and Ocean Bathymetry Mapping of Greenland From Multibeam Echo Sounding Combined With Mass Conservation. Geophysical Research Letters, 44(21), 11,051-11,061. https://doi.org/10.1002/2017GL074954

Morlighem, M., C. Williams, E. Rignot, L. An, J. E. Arndt, J. Bamber, G. Catania, N. Chauché, J. A. Dowdeswell, B. Dorschel, I. Fenty, K. Hogan, I. Howat, A. Hubbard, M. Jakobsson, T. M. Jordan, K. K. Kjeldsen, R. Millan, L. Mayer, J. Mouginot, B. Noël, C. O'Cofaigh, S. J. Palmer, S. Rysgaard, H. Seroussi, M. J. Siegert, P. Slabon, F. Straneo, M. R. van den Broeke, W. Weinrebe, M. Wood, and K. Zinglersen (2021). IceBridge BedMachine Greenland, Version 4. Boulder, Colorado USA. NASA National Snow and Ice Data Center Distributed Active Archive Center. https://doi.org/10.5067/VLJ5YXKCNGXO

Mouginot, J., Rignot, E., Bjørk, A. A., Broeke, M. van den, Millan, R., Morlighem, M., et al. (2019). Forty-six years of Greenland Ice Sheet mass balance from 1972 to 2018. Proceedings of the National Academy of Sciences, 116(19), 9239–9244. https://doi.org/10.1073/pnas.1904242116

Müller, L., Horwath, M., Scheinert, M., Mayer, C., Ebermann, B., Floricioiu, D., et al. (2021). Surges of Harald Moltke Bræ, north-western Greenland: seasonal modulation and initiation at the terminus. The Cryosphere, 15(7), 3355–3375. https://doi.org/10.5194/tc-15-3355-2021

Noël, B., van de Berg, W. J., Lhermitte, S., & van den Broeke, M. R. (2019). Rapid ablation zone expansion amplifies north Greenland mass loss. Science Advances, 5(9), eaaw0123. https://doi.org/10.1126/sciadv.aaw0123

Nuth, C., & Kääb, A. (2011). Co-registration and bias corrections of satellite elevation data sets for quantifying glacier thickness change. The Cryosphere, 5(1), 271–290. https://doi.org/10.5194/tc-5-271-2011

Oceans Melting Greenland. (2019). OMG Swath Gridded Multibeam Echo Sounding (MBES) Bathymetry. Ver. 1. PO.DAAC, CA, USA. https://doi.org/10.5067/OMGEV-MBES1

Porter, C., Morin, P., Howat, I., Noh, M.-J., Bates, B., Peterman, K., et al. (2018). ArcticDEM. Harvard Dataverse. https://doi.org/10.7910/DVN/OHHUKH

Robel, A. A., Pegler, S. S., Catania, G., Felikson, D., & Simkins, L. M. (2022). Ambiguous stability of glaciers at bed peaks. Journal of Glaciology, 1–8. https://doi.org/10.1017/jog.2022.31

Rignot, E., Xu, Y., Menemenlis, D., Mouginot, J., Scheuchl, B., Li, X., et al. (2016). Modeling of ocean-induced ice melt rates of five west Greenland glaciers over the past two decades. *Geophysical Research Letters*, *43*(12), 6374–6382. https://doi.org/10.1002/2016GL068784

Schlemm, T., & Levermann, A. (2021). A simple parametrization of mélange buttressing for calving glaciers. *The Cryosphere*, *15*(2), 531–545. https://doi.org/10.5194/tc-15-531-2021

Seale, A., Christoffersen, P., Mugford, R. I., & O'Leary, M. (2011). Ocean forcing of the Greenland Ice Sheet: Calving fronts and patterns of retreat identified by automatic satellite monitoring of eastern outlet glaciers. Journal of Geophysical Research: Earth Surface, 116(F3), F03013. https://doi.org/10.1029/2010JF001847

Shepherd, A., Ivins, E., Rignot, E., Smith, B., van den Broeke, M., Velicogna, I., et al. (2020). Mass balance of the Greenland Ice Sheet from 1992 to 2018. Nature, 579(7798), 233–239. https://doi.org/10.1038/s41586-019-1855-2

Slater, D. A., & Straneo, F. (2022). Submarine melting of glaciers in Greenland amplified by atmospheric warming. *Nature Geoscience*, 1–6. https://doi.org/10.1038/s41561-022-01035-9

Slater, D. A., Straneo, F., Das, S. B., Richards, C. G., Wagner, T. J. W., & Nienow, P. W. (2018). Localized Plumes Drive Front-Wide Ocean Melting of A Greenlandic Tidewater Glacier. Geophysical Research Letters, 45(22), 12,350-12,358. https://doi.org/10.1029/2018GL080763

Slater, Donald A., Felikson, D., Straneo, F., Goelzer, H., Little, C. M., Morlighem, M., et al. (2020). Twenty-first century ocean forcing of the Greenland ice sheet for modelling of sea level contribution. The Cryosphere, 14(3), 985–1008. https://doi.org/10.5194/tc-14-985-2020

Snow, T., Straneo, F., Holte, J., Grigsby, S., Abdalati, W., & Scambos, T. (2021). More than Skin Deep: Sea Surface Temperature as a Means of Inferring Atlantic Water Variability on the Southeast Greenland Continental Shelf Near Helheim Glacier. Journal of Geophysical Research: Oceans, 126(4), e2020JC016509. https://doi.org/10.1029/2020JC016509

Straneo, F., & Heimbach, P. (2013). North Atlantic warming and the retreat of Greenland's outlet glaciers. Nature, 504(7478), 36–43. https://doi.org/10.1038/nature12854

Sutherland, D. A., & Pickart, R. S. (2008). The East Greenland Coastal Current: Structure, variability, and forcing. Progress in Oceanography, 78(1), 58–77. https://doi.org/10.1016/j.pocean.2007.09.006

Sutherland, D. A., Straneo, F., Stenson, G. B., Davidson, F. J. M., Hammill, M. O., & Rosing-Asvid, A. (2013). Atlantic water variability on the SE Greenland continental shelf and its relationship to SST and bathymetry. Journal of Geophysical Research: Oceans, 118(2), 847–855. https://doi.org/10.1029/2012JC008354

Todd, J., & Christoffersen, P. (2014). Are seasonal calving dynamics forced by buttressing from ice mélange or undercutting by melting? Outcomes from full-Stokes simulations of Store Glacier, West Greenland. The Cryosphere, 8(6), 2353–2365. https://doi.org/10.5194/tc-8-2353-2014

Todd, Joe, Christoffersen, P., Zwinger, T., Råback, P., Chauché, N., Benn, D., et al. (2018). A Full-Stokes 3D Calving Model applied to a large Greenlandic Glacier. Journal of Geophysical Research: Earth Surface. https://doi.org/10.1002/2017JF004349

Todd, Joe, Christoffersen, P., Zwinger, T., Råback, P., & Benn, D. I. (2019). Sensitivity of a calving glacier to ice—ocean interactions under climate change: new insights from a 3-D full-Stokes model. The Cryosphere. https://doi.org/10.5194/tc-13-1681-2019

Walsh, K. M., Howat, I. M., Ahn, Y., & Enderlin, E. M. (2012). Changes in the marine-terminating glaciers of central east Greenland, 2000–2010. The Cryosphere, 6(1), 211–220. https://doi.org/10.5194/tc-6-211-2012

Walter, F., O'Neel, S., McNamara, D., Pfeffer, W. T., Bassis, J. N., & Fricker, H. A. (2010). Iceberg calving during transition from grounded to floating ice: Columbia Glacier, Alaska. Geophysical Research Letters, 37(15). https://doi.org/10.1029/2010GL043201

Walter, J. I., Box, J. E., Tulaczyk, S., Brodsky, E. E., Howat, I. M., Ahn, Y., & Brown, A. (2012). Oceanic mechanical forcing of a marine-terminating Greenland glacier. Annals of Glaciology, 53(60), 181–192. https://doi.org/10.3189/2012AoG60A083

Williams, J. J., Gourmelen, N., Nienow, P., Bunce, C., & Slater, D. (2021). Helheim Glacier Poised for Dramatic Retreat. Geophysical Research Letters, 48(23), e2021GL094546. https://doi.org/10.1029/2021GL094546

Wood, M., Rignot, E., Fenty, I., Menemenlis, D., Millan, R., Morlighem, M., et al. (2018). Ocean-Induced Melt Triggers Glacier Retreat in Northwest Greenland. Geophysical Research Letters, 45(16), 8334–8342. https://doi.org/10.1029/2018GL078024

Wood, Michael, Rignot, E., Fenty, I., An, L., Bjørk, A., Broeke, M. van den, et al. (2021). Ocean forcing drives glacier retreat in Greenland. Science Advances, 7(1), eaba7282. https://doi.org/10.1126/sciadv.aba7282

Xu, Y., Rignot, E., Fenty, I., Menemenlis, D., & Flexas, M. M. (2013). Subaqueous melting of Store Glacier, west Greenland from three-dimensional, high-resolution numerical modeling and ocean observations. *Geophysical Research Letters*, *40*(17), 4648–4653. https://doi.org/10.1002/grl.50825

Supplement to 'Atlantic Water intrusion triggers rapid retreat and regime change at previously stable Greenland glacier'

Chudley, T. R.[1]*, Howat, I. M.[1,2], King, M. D.[3], Negrete, A.[1]

[1] Byrd Polar and Climate Research Center, Ohio State University, Columbus, OH, USA
[2] School of Earth Sciences, Ohio State University, Columbus, OH, USA
[3] Polar Science Center, University of Washington, Seattle, WA, USA

Correspondence: Tom Chudley (chudley.1@osu.edu)

Supplementary Text

Supplementary Figures 1 – 8

Supplementary Tables 1 – 2

Supplementary Text

Accuracy of bed data at Steenstrup

BedMachine v4 data reports that the front ~600 m of Steenstrup (based on 2016 terminus position) is ~20 m above sea level (fig. 3a), a value that is patently unphysical. BedMachine v4 data source values indicate that no mass conversation was applied in the sector, and the bed depth was inferred solely from krigging of input data. Hence, we suggest that the anomaly is likely due to the fact that OMG MBES data for Steenstrup, which is incorporated into BedMachine (Morlighem *et al.*, 2017), includes the calving face within the bathymetry data (OMG, 2016; fig. S3a), which is thus misinterpreted to become an erroneous sea-level anomaly in synthesised datasets. Manual inspection of the OMG MBES data suggests that the true depth of the calving front lies in the range ~300-360 m, based upon which we suggest the foremost ~1.8 km of the bed profile is unreliable (fig. 3a).

To further investigate the reliability of the gridded data, we examine Operation IceBridge Multichannel Coherent Radar Depth Sounder (MCoRDS) airborne flight lines (Paden *et al.* 2010), which were also incorporated into the final product (fig S7). These suggest that our estimation of the extent of unreliable BedMachine extent is accurate, but also that BedMachine data within ~13 km of the 2016 terminus is likely reasonable. This supports our assessment that a retrograde bedslope is likely a positive feedback influencing the rapid 2018-2021 retreat. However, with the bed between ~13 – ~22 km upstream being poorly resolved in the MCoRDS data, the future influence of the bed geometry on Steenstrup's retreat is uncertain.

Our finding that Steenstrup's front depth is underestimated in BedMachine v4 is consistent with Millan et al. (2018), who integrate high-resolution OMG airborne gravimetry data to show that glaciers in SE GrIS have fjords hundreds of metres deeper than shown in BedMachine v3, and fewer shallow sills that limit access to AW. These erroneous data exist even though Steenstrup has a surprising amount of observations for a previously unremarkable glacier, including multiple IceBridge MCoRDS repeats and OMG MBES data. Many other glaciers suffer from a lack of observations entirely. Glaciers with notably long trunks bounded by valleys (typical for the south and central eastern sectors) are poorly represented by BedMachine due to a lack of observational data, with reported thicknesses no greater than tens of metres despite moving at a rates in excess of several metres per day. Named glaciers with these errors include Glacier de France (66.44°N, 35.92°W), Tasilaq Glacier (66.71°N, 34.30°W), and Nordre Parallelgletscher (67.77°N, 33.36°W). It is likely that the current literature, working largely from Greenland-wide synthesis datasets such as BedMachine, has underidentified vulnerable marine-terminating glaciers, with many other previously stable glaciers such as Steenstrup still potentially vulnerable.

References not in main text

OMG (2016). Oceans Melting Greenland Bathymetric Survey - South East Greenland 2016 Operations Report: Appendix A - Daily Field Reports. https://podaac-tools.jpl.nasa.gov/drive/files/allData/omg/L2/docs/2016/Appendix_A-Daily_Reports.pdf

Paden, J., J. Li, C. Leuschen, F. Rodriguez-Morales, and R. Hale. (2010). IceBridge MCoRDS L2 Ice Thickness, Version 1. Boulder, Colorado USA. NASA National Snow and Ice Data Center Distributed Active Archive Center. https://doi.org/10.5067/GDQ0CUCVTE2Q

Supplementary Figures

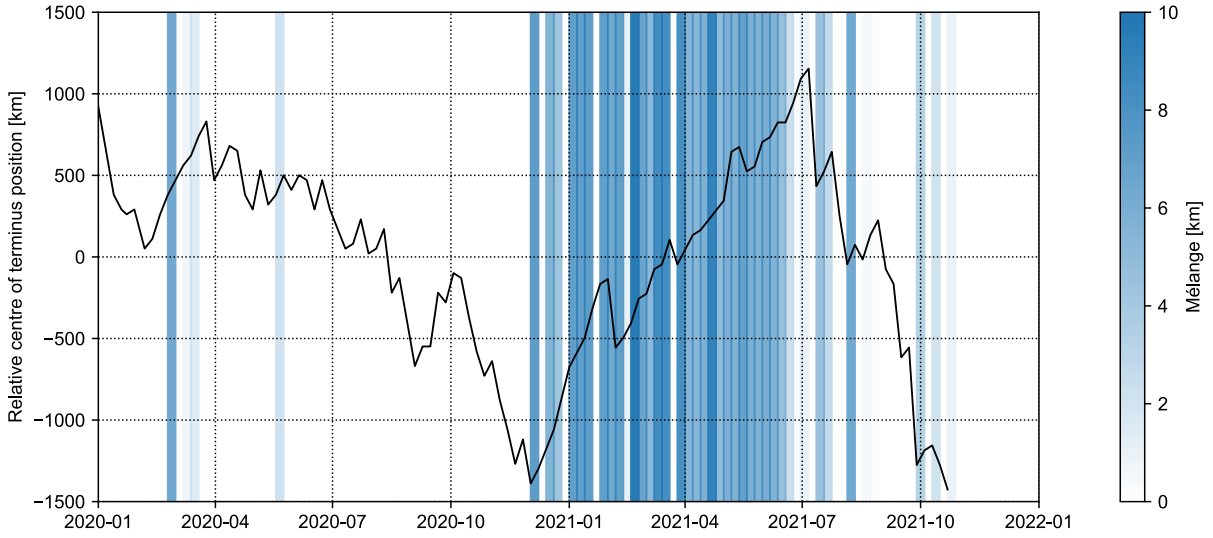

Figure S1: *Expanded version of fig. 2b showing terminus position (black line) and mélange presence and extent (blue shading) in 2020 and 2021.*

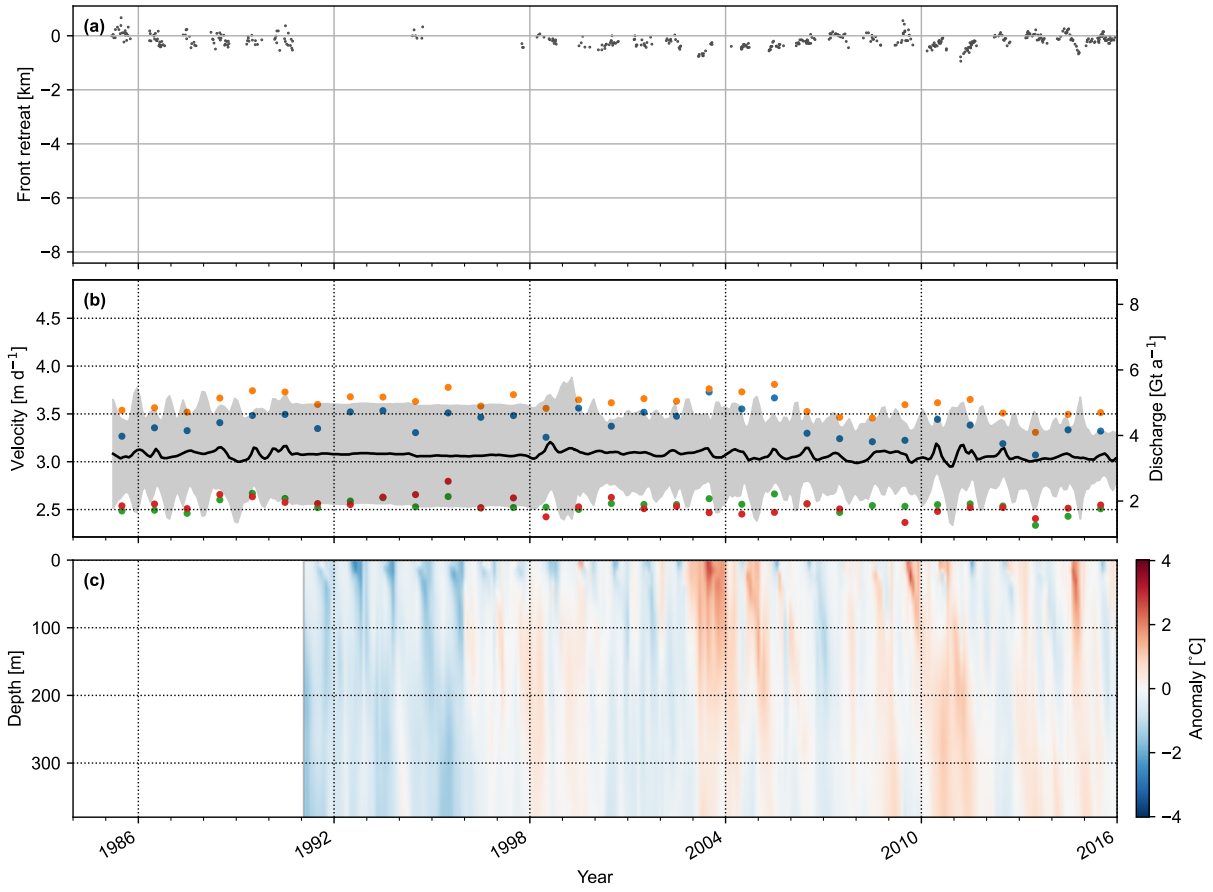

Figure S2: *Expanded version of figures 2a, 2c, and 2e, showing (a) front position; (b) discharge and annual mean velocity, and (c) CMEMS monthly mean ocean temperature anomaly between 1985 and 2016.*

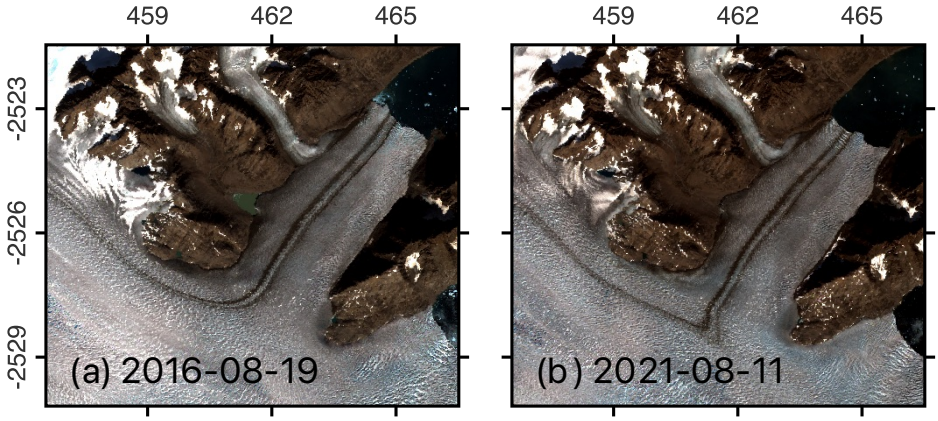

Figure S3: *Sentinel-2 imagery showing displacement of the medial moraine of the northern distributary of Steenstrup between 2016 and 2021 as flow is captured by the main trunk. Coordinates in units km of NSIDC Sea Ice Polar Stereographic North (EPSG:3413).*

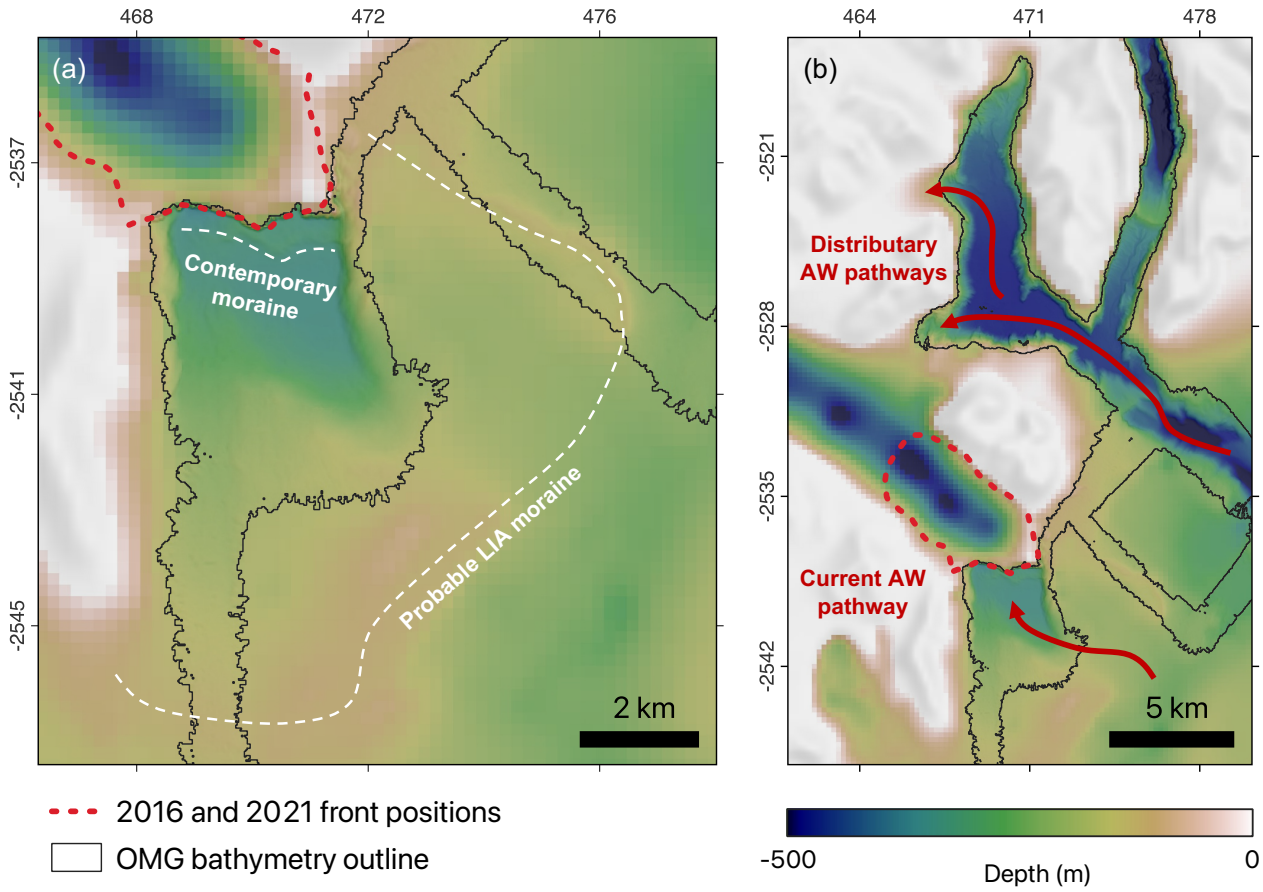

Figure S4: *(a) Hillshaded bathymetric data in front of Steenstrup from IBCAO v4 (which draws subglacial topography from BedMachine) and OMG MBES data. White dashed lines mark the contemporary and Little Ice Age (LIA) moraines identified by Batchelor* et al. *(2019). NB the artificial sea-level topography introduced into BedMachine at the 2016 terminus position due to OMG MBES incorporation of the calving front. (b) Potential alternative AW pathways through the distributaries. NB the inability of BedMachine to resolve ice depth at the northern distributary.*

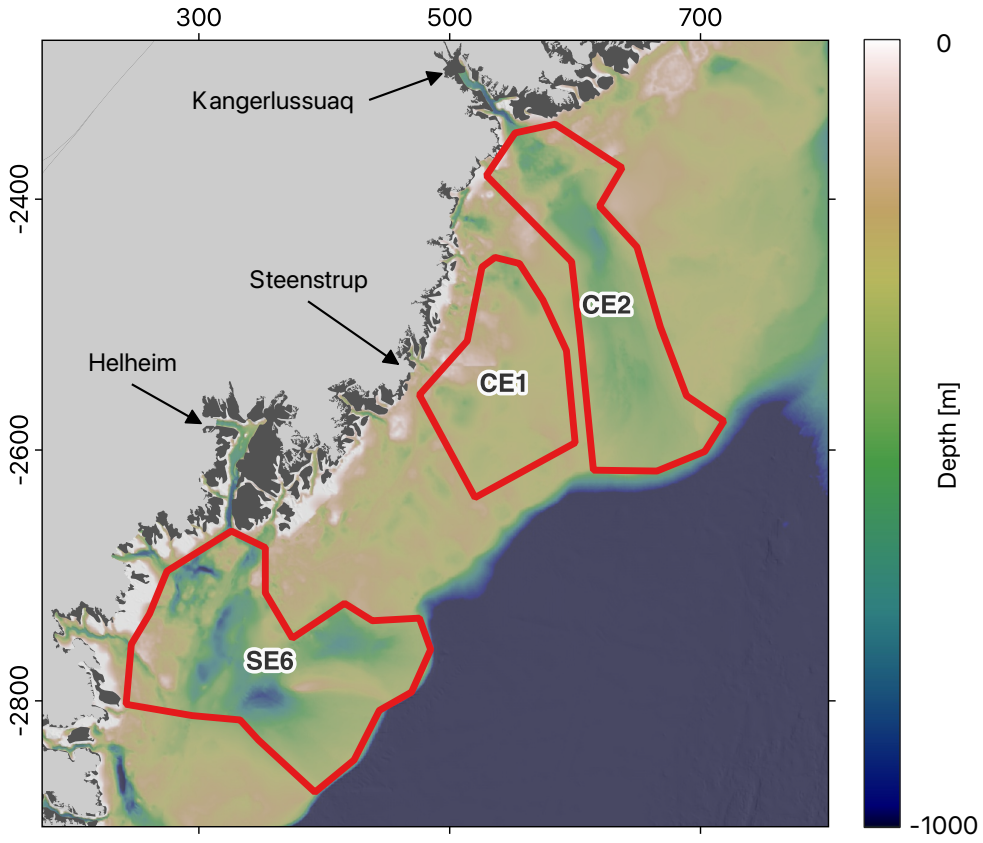

Figure S5: *Location of Wood* et al. *(2021) sample zones. Background is hillshaded IBCAO bathymetry. Coordinates are in units km of NSIDC Sea Ice Polar Stereographic North (EPSG:3413).*

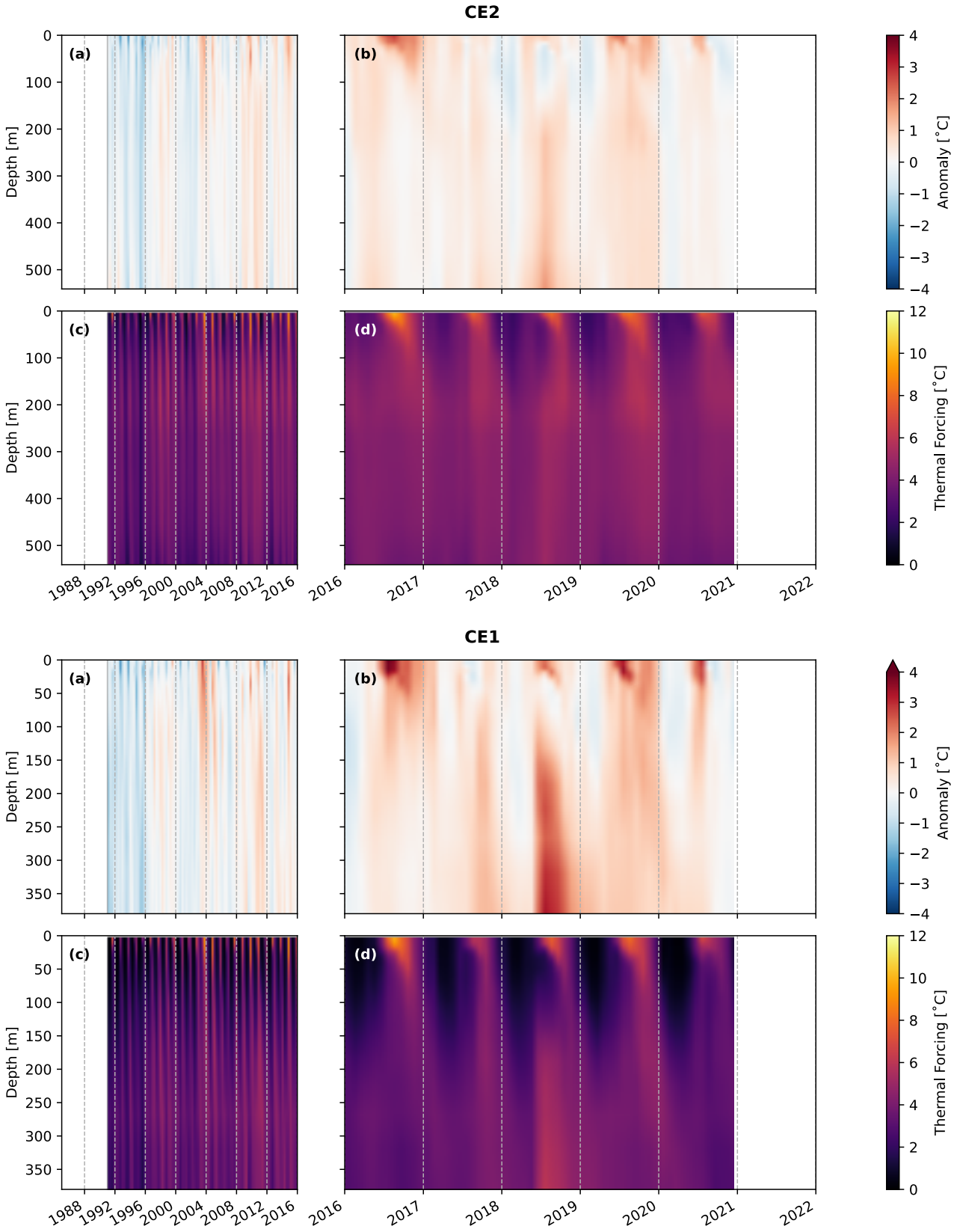

Figure S6: *Ocean temperature anomaly and thermal forcing for each of the CE2, CE1, and SE6 sample zones from Wood* et al. *(2021). For each subfigure: (a) Temperature anomaly from the 1992-2021 mean between 1992 and 2015. (b) Temperature anomaly from the 1992-2021 mean between 2016 and 2021. (c) Thermal forcing between 1992 and 2015. (d) Thermal forcing between 2016 and 2021.* ***(continues on next page)***

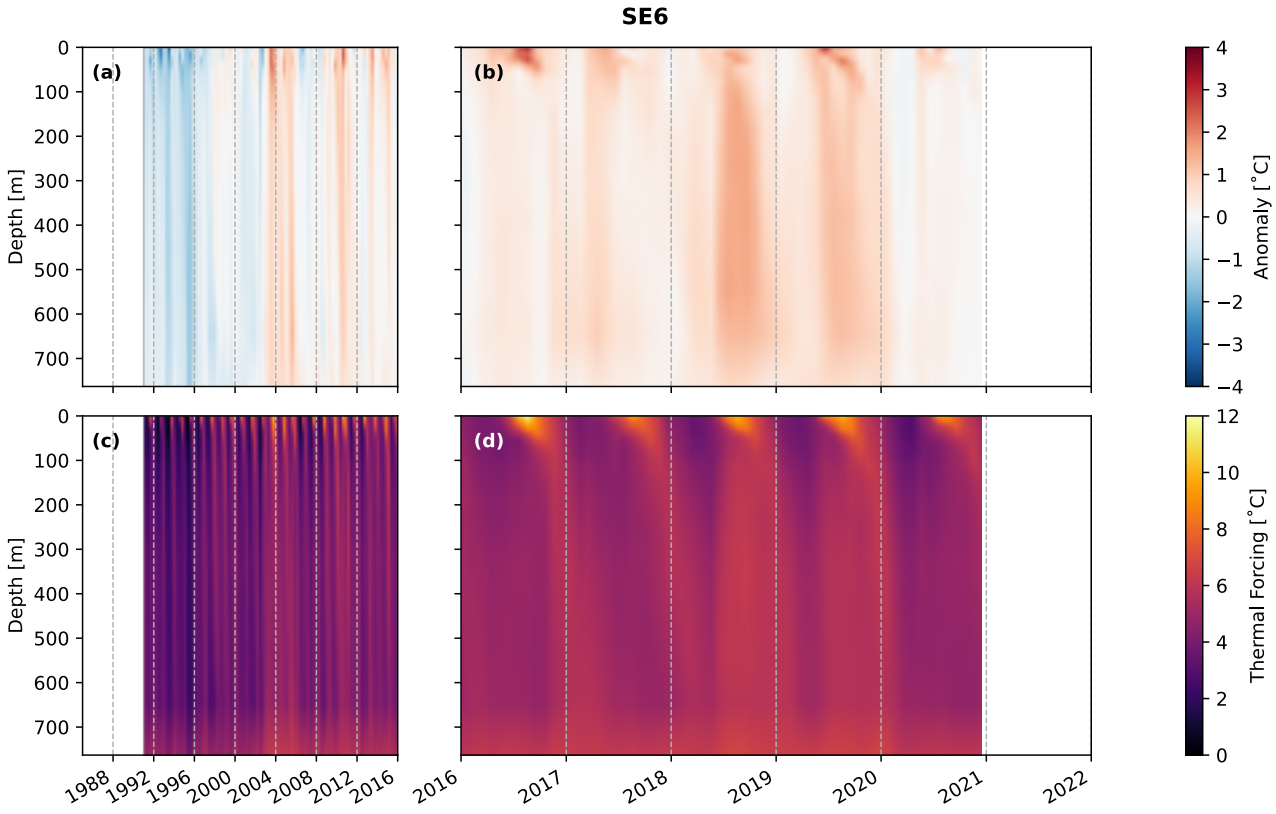

Figure S6: *(continued)*

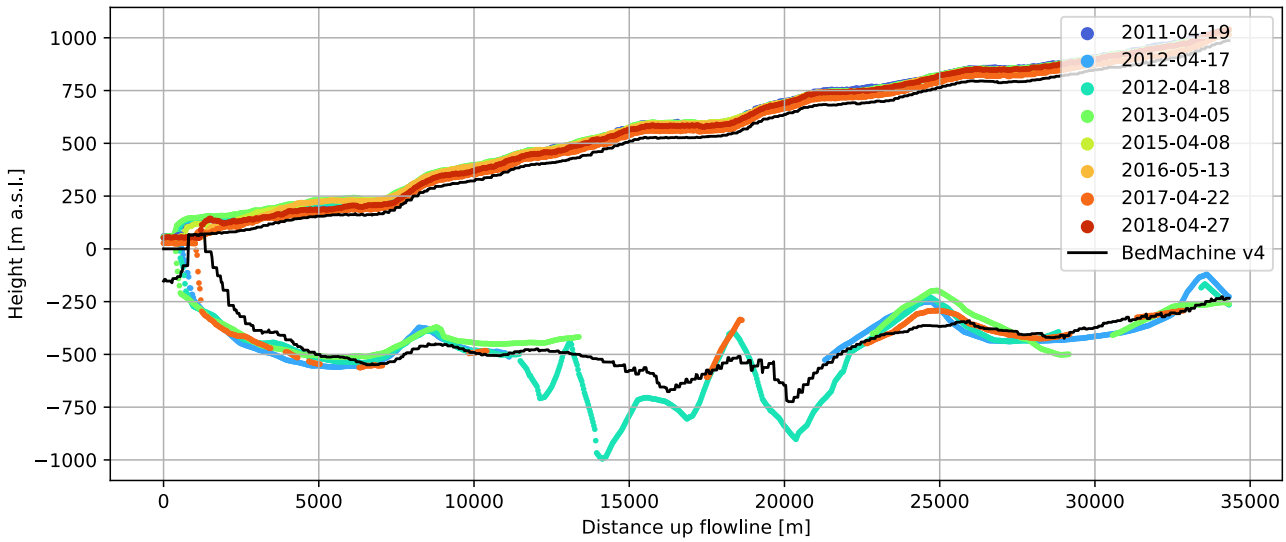

Figure S7: *Airborne MCoRDS data (Paden* et al. *2010) visualising the surface and bed returns in comparison to BedMachine v4 data (black line).*

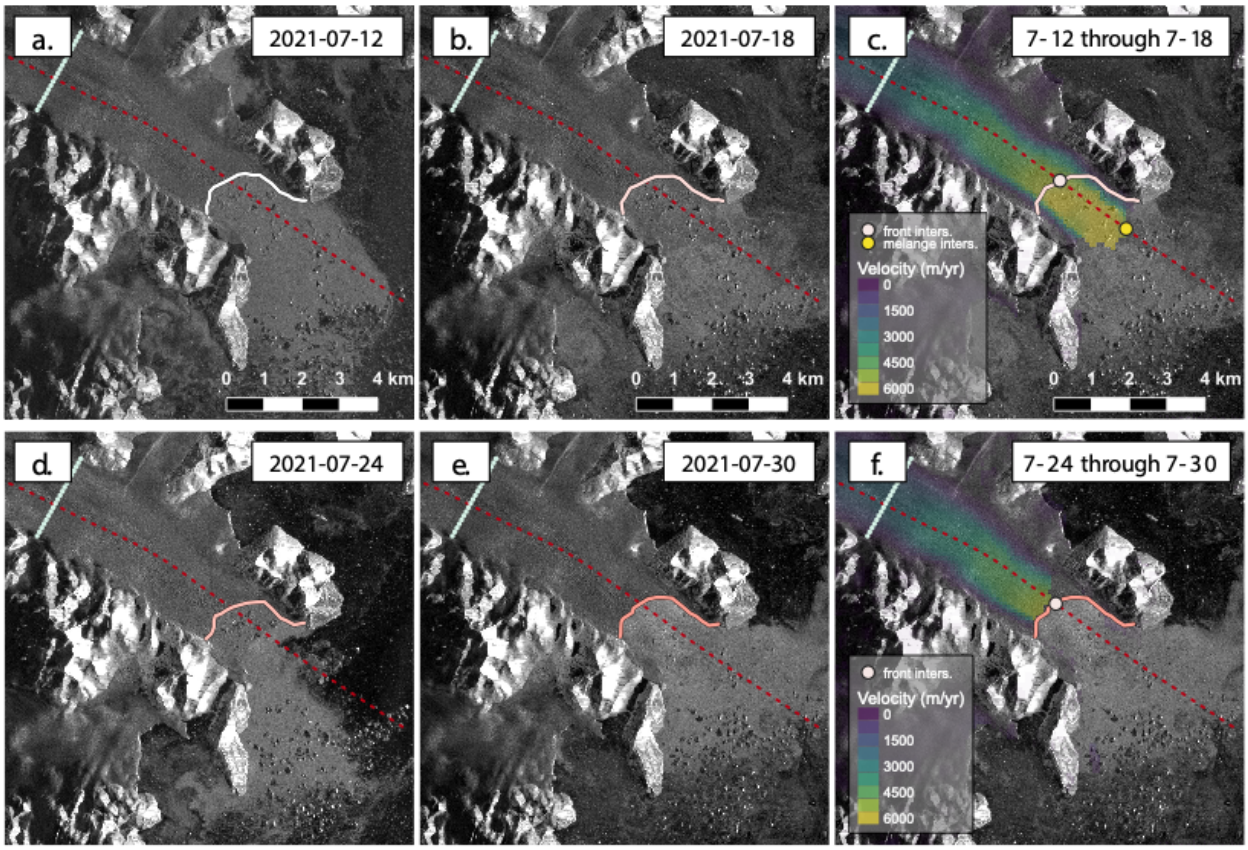

Figure S8: *Consecutive Sentinel-1 images for July 12th, 2021 (a) and July 18th, 2021 (b), and the corresponding velocity map between the two images in (c). The flux gate measurements coordinates are plotted upstream in light green, as well as an extended center flowline as the dashed red line. The terminus position in each image is also delineated in white to pink shades with time, with circled markers indicating the intersection between both the terminus and outer extent of rigid melange with the center flowline. Unlike the proglacial rigid melange shown in (c), velocity mapping between July 24 (d) and 30th (e) indicate the melange decorrelates between successive images and is nonrigid (f).*

Supplementary Tables

Table S1: *Positions of sampling points presented in Fig 1a and Fig 2b, in coordinates of NSIDC Sea Ice Polar Stereographic North (EPSG:3413).*

Point	**X**	**Y**
a	464895	-2533001
b	460732	-2530257
c	456475	-2527582
d	451777	-2526768

Table S2: *Date and IDs of ArcticDEM strips used*

Date	**ArcticDEM 2m Strip**
2016-03-27	WV01_20160327_102001004BC7AC00_102001004AC12E00_2m_lsf
2016-04-04	WV01_20160404_102001004AA8F800_102001004D67D900_2m_lsf
2016-08-03	WV01_20160803_1020010054389200_10200100537DE100_2m_lsf
2017-06-07	WV01_20170607_1020010063D4CE00_10200100617E7F00_2m_lsf
2017-08-05	WV01_20170805_1020010065C0F200_102001006260ED00_2m_lsf
2018-04-05	WV01_20180405_1020010072328700_102001007149E600_2m_lsf
2018-04-23	WV03_20180423_104001003A7FE400_104001003A9F3100_2m_lsf
2018-05-30	WV03_20180530_104001003DC69400_104001003E486E00_2m_lsf
2019-05-11	WV03_20190511_104001004BBA4500_104001004C5DCC00_2m_lsf
2019-06-14	WV01_20190614_102001008B302C00_1020010087237C00_2m_lsf
2019-07-22	WV01_20190722_1020010086AC6800_1020010085418C00_2m_lsf
2020-07-09	WV01_20200709_102001009A689B00_102001009B63B200_2m_lsf
2020-07-14	WV01_20200714_102001009BEB8300_102001009CB09500_2m_lsf
2021-07-31	WV02_20210731_10300100C359CF00_10300100C37C8000_2m_lsf
2021-08-14	WV02_20210814_10300100C3611400_10300100C4831700_2m_lsf